ACS Infectious Diseases

pubs.acs.org/journal/aidcbc

Article

Oxadiazolone Derivatives: Powerful Tools to Reduce *Staphylococcus aureus* Infection

Emma Forest, Jordan Lehoux, Léo Faion, David Ranava, Virginie Mohymont, Thierry Durand, Stéphane Audebert, Luc Camoin, Céline Crauste, Stéphane Canaan, Jean Michel Brunel, Françoise Van Bambeke, Jean-Michel Bolla,* and Jean-François Cavalier*

Cite This: https://doi.org/10.1021/acsinfecdis.6c00165

Read Online

ACCESS | Metrics & More | Article Recommendations | Supporting Information

ABSTRACT: *Staphylococcus aureus* is a Gram-positive opportunistic pathogen and a top priority bacterium in the fight against antimicrobial resistance. Its high propensity to develop resistance, its high virulence, and its ability to form biofilms and persist intracellularly result in difficult-to-treat infections against, which new chemical classes are urgently needed. Here, we investigated the antibacterial activity of oxadiazolone-core derivatives (**OX**) against planktonic, intracellular, and biofilm-associated *S. aureus*. Among the tested compounds, **M*p*PPOX** exhibited a bactericidal effect on extracellular bacteria with an MIC similar to that of vancomycin; **iBPOX** mainly inhibited intracellular replication, while **HPOX** strongly impaired initial biofilm formation. These results prompted us to identify the potential target enzymes of the three **OXs** via activity-based protein profiling, combined with mass spectrometry. The antibiofilm **HPOX** compound was indeed found to primarily react with enzymes involved in biofilm formation and associated virulence, while **iBPOX** and the most active **M*p*PPOX** inhibitor targeted multiple (Ser/Cys)-based enzymes. Among these, the FabH protein has been confirmed as a vulnerable target of **M*p*PPOX**. Overall, this study underscores the multitarget nature of the **OXs**, which covalently bind to several (Ser/Cys)-based enzymes of interest. Such property makes them highly versatile chemotypes that could be used as broad-spectrum antimicrobial agents, notably by improving the antibiofilm activity of ineffective or poorly active drugs.

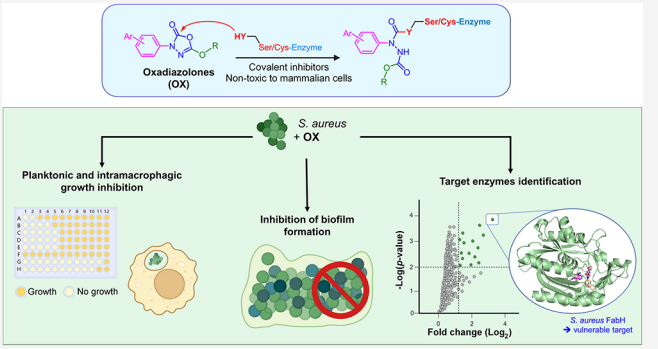

KEYWORDS: *Gram-positive bacteria, antibiotic resistance, antibiofilm activity, activity-based protein profiling, multitarget inhibitors, FabH*

The "Golden Era" of antibiotics, which spanned from the 1940s to the 1960s, drastically changed our relationship with bacteria. The large number of new drugs discovered during this period offered the healthcare community hope by enabling life-threatening infections to be cleared within a few days of treatment.[1,2]

However, prescription policies, both in human and veterinary health, led to the swift emergence of antimicrobial resistance (AMR) among bacterial populations, which became a public health concern. As of today, multiple studies have shed light on the alarming numbers of AMR-related deaths, which amounted to 1.14 million in 2021, with an additional 4.71 million associated with it.[3] In the context of AMR, *Staphylococcus aureus* exhibits remarkable virulence and colonization capabilities, mainly due to its various toxins and its ability to form biofilms. According to the WHO, *S. aureus* is responsible for the largest increase in deaths, which rose from 103,000 in 1990 to 196,000 in 2021,[3] thus remaining a high-priority human pathogen.[4,5] In particular, methicillin-resistant *S. aureus* (MRSA), along with *Escherichia coli*, has been deemed responsible for >50% of the fatal burden attributed to AMR.[6] Among resistance mechanisms used by *S. aureus*, biofilms act as major protection against environmental and chemical stresses.[7,8] These multicellular structures, composed of several bacterial layers embedded in a thick extracellular polymeric substance (EPS), act as a mechanical barrier that slows down antibiotics diffusion and limits the efficiency of host phagocytosis.[9,10] Reduced growth metabolic rates and bacterial dormancy within biofilms are also known to increase antibiotic tolerance.[11,12] Additionally, biofilms facilitate horizontal gene transfer, thereby promoting the spread of resistance mechanisms.[13−15] The rapid emergence of AMR in *S. aureus* outpaces the development of new

Received: February 16, 2026
Revised: April 3, 2026
Accepted: April 29, 2026

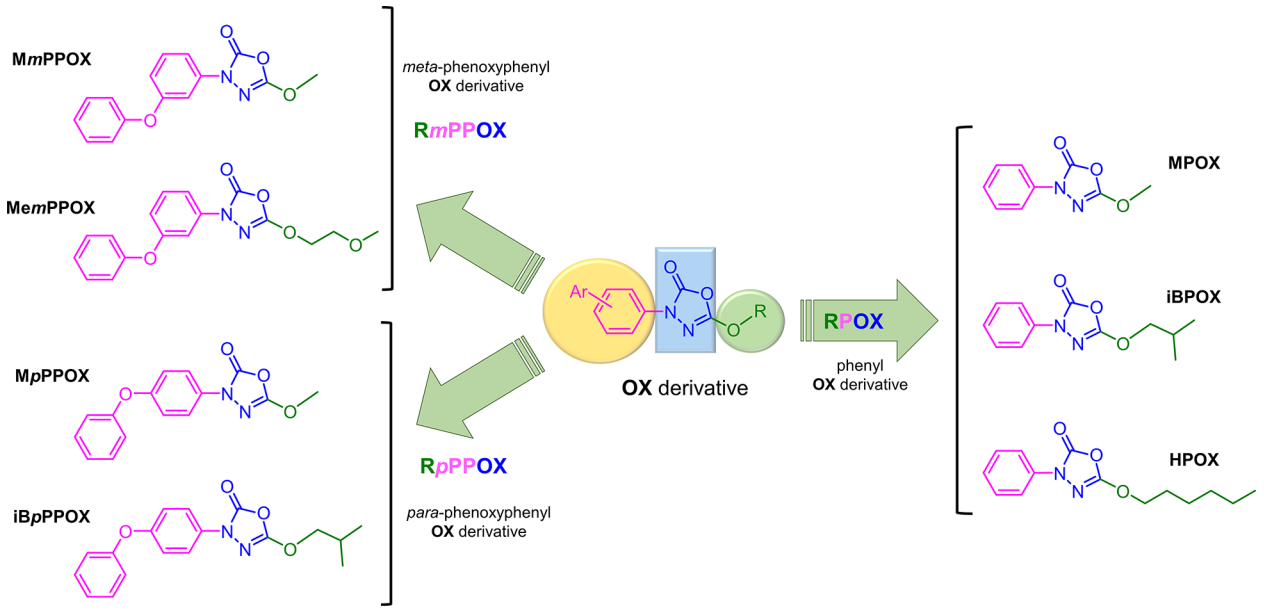

Figure 1. Chemical structures of oxadiazolone-core (**OX**) derivatives.[20,23,24]

antimicrobials, thereby posing a significant global challenge. With resistant strains frequently identified and few new treatments available, some studies predict that AMR could cost over 100 trillion dollars per year by 2050.[16]

In this context, multitarget compounds are emerging as a promising strategy for overcoming this critical public health issue, as they can prevent the development of target-specific resistance.[17−19]

Several years ago, we developed and characterized a family of multitarget inhibitors, the oxadiazolones-core derivatives (**OX**).[20,21] The **OX** are suicide inhibitors that form a covalent bond with the catalytic serine or cysteine residues in the active site of target proteins, resulting in the inhibition of the enzymatic activity of these (Ser/Cys)-based enzymes.[20,21] The **OX** also demonstrated great promise as antimycobacterial agents, leading to the inhibition of mycobacterial growth while remaining nontoxic to mammalian cells. Indeed, although inactive against Gram-negative bacteria,[22] our **OXs** were found to inhibit the extracellular and intracellular growth of *Mycobacterium abscessus*[23] and *Mycobacterium tuberculosis*[24] by impairing the activity of various (Ser/Cys)-based enzymes involved in important physiological processes linked to mycobacterial lipids (cholesterol and free fatty acid) and cell wall biosynthesis.[21,23,24]

More recently, oxadiazolone-based electrophile warheads have been reported to exhibit high antibacterial potency against the multidrug-resistant *S. aureus* MRSA strain USA300.[25−27] Using an alkyne-based probe (ABP) derivative of the most potent optimized hit from the MRSA screening, the authors identified the FphB and FphC serine hydrolases[25,27] and the highly conserved fatty acid synthesis II (FASII) pathway enzyme FabH[28] as effective targets.

Given all these previous findings, in the present study we have further assessed the effect of 7 selected **OXs** derivatives (i.e., **MpPPOX**, **MemPPOX**, **MmPPOX**, **iBpPPOX**, **MPOX**, **HPOX**, **iBPOX**, Figure 1) against *S. aureus* growth: planktonic, biofilm-associated, or inside infected THP-1-derived macrophages. Among them, **MpPPOX** showed MIC values similar to vancomycin or linezolid and a significant bactericidal activity against planktonic *S. aureus*. On the other hand, **HPOX** exhibited a highly specific antiadhesive activity, blocking biofilm formation at concentrations down to 0.01 × MIC. Converting these latter **OXs** to ABPs enabled the direct capture of their respective target enzymes via click-chemistry activity-based protein profiling (CC-ABPP). Proteomics analysis further identified these captured proteomes, which correlated with the observed activities of the two molecules. Among these potential targets, the β-ketoacyl-[acyl-carrier-protein] synthase III (FabH) protein has been confirmed as a vulnerable target of **MpPPOX.**

RESULTS AND DISCUSSION

OX Compounds Impair the Planktonic Growth of *S. aureus* Reference Strain and Clinical Isolates

The antimicrobial activities of the seven selected **OXs** (Figure 1), previously described as active against several pathogenic mycobacteria such as *M. tuberculosis*[24] or *M. abscessus*,[23] have been tested against planktonic *S. aureus* ATCC 25923 reference strain. Their minimal inhibitory concentrations (MICs) leading to 50% and 90% growth inhibition, referred to as MIC_{50} and MIC_{90}, respectively, were determined using the rapid *p*-iodonitrophenyltetrazolium violet (INT) colorimetric assay following absorbance readings at 470 nm.[22,29,30]

As shown in Table 1, the tested compounds displayed distinct antibacterial activities against the growth of *S. aureus* ATCC 25923. First, **iBpPPOX** was completely inactive (MIC_{50} > 128 μg/mL) and **MPOX** exhibited only moderate activity (MIC_{50} ~31.1 ± 5.2 μg/mL). In contrast, the remaining five **OXs** were able to efficiently block 50% of *S. aureus* planktonic growth with MIC_{50} values comparable to those of clinically relevant antibiotics, such as vancomycin (VAN; MIC_{50}~1.1−2.2 μg/mL) and linezolid (LZD; MIC_{50} ~0.13−0.17 μg/mL). Their efficacy can be ranked as follows: **MmPPOX** (0.92 ± 0.37 μg/mL) ≈ **MpPPOX** (1.3 ± 0.14 μg/mL) > **iBPOX** (2.1 ± 0.54 μg/mL) ≈ **HPOX** (2.7 ± 0.70 μg/mL) > **MemPPOX** (5.6 ± 1.9 μg/mL).

The determination of the MIC_{90} values further provided a clear assessment of the antibacterial activity of these compounds. **MmPPOX** (3.3 ± 1.14 μg/mL) and **MpPPOX**

https://doi.org/10.1021/acsinfecdis.6c00165
ACS Infect. Dis. XXXX, XXX, XXX−XXX

Table 1. Antibacterial Activities of Selected OXs against *S. aureus* ATCC 25923 and SH1000 Reference Strains[a]

	MIC_{50} | MIC_{90} (μg/mL)	
compound	ATCC 25923	SH1000
iBPOX	2.1 ± 0.54 | 65.3 ± 3.5	1.5 ± 0.97 | 50.7 ± 4.8
iB*p*PPOX	>128	
HPOX	2.7 ± 0.70 | >128	2.2 ± 0.94 | >128
MPOX	31.1 ± 5.2 | >128	
M*p*PPOX	1.3 ± 0.14 | 5.9 ± 1.4	0.34 ± 0.16 | 2.1 ± 0.57
M*m*PPOX	0.92 ± 0.37 | 3.3 ± 1.1	
Me*m*PPOX	5.6 ± 1.9 | >128	
LZD	0.17 ± 0.02 | 1.1 ± 0.07	0.13 ± 0.08 | 2.0 ± 0.72
VAN	1.1 ± 0.24 | 1.5 ± 0.24	2.2 ± 0.69 | 2.6 ± 0.94

[a]$MIC_{50/90}$: compound concentration leading to 50/90% of growth inhibition, determined by the INT assay following an absorbance reading at 470 nm. Values are the mean values of three independent assays performed in triplicate. LZD, linezolid; VAN, vancomycin; and reference drugs.

(5.9 ± 1.4 μg/mL) emerged as the most potent inhibitors of *S. aureus* ATCC 25923 growth, while **iBPOX** (65.3 ± 3.5 μg/mL) displayed a moderate MIC_{90} value. The remaining **OXs** had MIC_{90} values >128 μg/mL, despite strong MIC_{50}s for **HPOX** and **Me*m*PPOX** (Table 1).

To better understand the discrepancy in the antibacterial activity (i.e., MIC_{90}) of our compounds, we decided to focus on three **OX** derivatives: **HPOX** (poorly active), **iBPOX** (moderately active), and **M*p*PPOX** (highly active) and investigated their antibacterial activity on various *S. aureus* strains.

First, similar MIC_{50} and MIC_{90} values were observed when the three **OXs** were tested against the methicillin-sensitive *S. aureus* SH1000 strain compared to the ATCC 25923 reference strain (Table 1).[31] In contrast, when tested against *S. aureus* clinical isolates[32] (Table 2), two different inhibition profiles were obtained depending on the isolates' origin (Table S1). *SA005* and *SA006,* isolated from blood and pus, respectively, and exhibiting resistance to a single antibiotic, were nearly 1.3- to 5.6-times less sensitive to the **OXs** than the ATCC 25923 and SH1000 strains. Conversely, the clinical MRSA strains *SA002, SA003,* and *SA009* obtained from patients' sputum, exhibited greater susceptibility to the three **OXs** despite their high antibiotic resistance profiles (Table S1). The most significant gain in MICs is achieved with **HPOX**, with a 49- to 144-fold improvement in MIC_{90} as compared to reference strains. Similar trends were also obtained with **iBPOX** (5.6- to 14.5-fold decrease in MIC_{90}) and **M*p*PPOX** (7.2- to 24.6-fold decrease in MIC_{90}). This latter compound still remained a potent inhibitor of all *S. aureus* strains tested.

Although the observed disparities in antimicrobial susceptibility among *S. aureus* clinical isolates cannot be directly correlated with their respective resistance profile (Table S1), the isolates' origin[32] may however provide clues to explain them. Indeed, bacteria isolated from patients' sputum (*SA002*, *SA003*, and *SA009*) are often chronically colonizing bacteria that undergo phenotypic changes, display reduced virulence, and tend to form biofilms. This is less common in acute infections, such as bacteremia (*SA005*) or pus (*SA006*). However, an arbitrary strain-dependent variability toward the **OXs** cannot be excluded, and further investigations (genomic/lipidomic/transcriptomic/proteomic···) into strain-to-strain differences should be needed to explain the discrepancy in susceptibility to the three **OXs** among the five clinical strains tested.

OXs Exhibit Antibacterial Activity against Planktonic and/or Intramacrophagic Growth of *S. aureus*

A time-kill assay was further performed to evaluate the bactericidal or bacteriostatic nature of the three selected **OXs** as compared to vancomycin (VAN) used as a reference drug (Figure 2A,B). The bacteria were incubated with **HPOX**, **iBPOX**, **M*p*PPOX**, or vancomycin at their respective MIC_{90} for 24 h. In the case of **HPOX**, a 128 μg/mL concentration was arbitrary used in these assays. Samples were then taken at various time intervals and spread onto agar plates for colony-forming units (CFUs) count. The results clearly show that the three **OXs** displayed distinct behaviors consistent with their respective antibacterial activity. Indeed, **HPOX** was only found to delay *S. aureus* growth by 6−8 h, while **iBPOX** induced a significant 3-Log reduction in CFU count after 24 h incubation compared to the controls (Figure 2A). Increasing the concentrations to 256 μg/mL (**HPOX**) or 2 × MIC_{90} (**iBPOX**) did not change the overall time-kill curve profile of these two compounds (Figure S1A). However, it failed to block bacterial growth, with a ∼2.5-Log increase in the CFU count compared to the initial inoculum (t = 0) (Figure 2B). In contrast, with a 7-Log reduction in CFU count after 24 h (Figure 2A) and a 1.3-Log decrease compared to the initial inoculum (Figure 2B), **M*p*PPOX** displayed a constant killing effect against planktonic *S. aureus*. Increasing its concentration up to 5 × MIC_{90} (∼29.5 μg/mL) confirmed this trend, resulting in a similar bactericidal profile to vancomycin and achieving a 3-Log reduction in CFU counts compared to the initial inoculum (Figure S1B,C).

It is now accepted that *S. aureus* can invade and replicate inside eukaryotic phagocytic cells.[33,34] Such infected cells act as a "Trojan horse" allowing dissemination, and the intracellular bacteria mainly contribute to the chronic nature of staphylococcal infections, relapsing disease, and antibiotic treatment failure.[33,35] The fact that the **OXs** were also able to inhibit the growth of *M. abscessus* and *M. tuberculosis* inside infected macrophages,[21,23,24] prompted us to investigate their effects

Table 2. Antibacterial Activities of the Three Selected OXs against *S. aureus* Clinical Isolates[a]

	MIC_{50} | MIC_{90} (μg/mL)				
compound	*SA002*	*SA003*	*SA005*	*SA006*	*SA009*
iBPOX	2.1 ± 0.54 | 8.5 ± 1.3	1.5 ± 0.19 | 11.6 ± 1.9	7.5 ± 1.3 | >128	11.7 ± 0.75 | >128	0.90 ± 0.21 | 4.5 ± 0.19
HPOX	0.88 ± 0.09 | 2.6 ± 0.03	0.61 ± 0.08 | 1.7 ± 0.24	7.2 ± 3.2 | >128	5.4 ± 0.94 | >128	0.43 ± 0.08 | 0.89 ± 0.08
M*p*PPOX	0.39 ± 0.10 | 0.57 ± 0.15	0.38 ± 0.10 | 0.82 ± 0.11	2.2 ± 1.3 | 7.9 ± 1.8	2.5 ± 0.30 | 8.6 ± 2.1	0.20 ± 0.04 | 0.24 ± 0.09
VAN	0.57 ± 0.03 | 0.68 ± 0.03	0.60 ± 0.01 | 0.87 ± 0.27	0.59 ± 0.002 | 0.70 ± 0.03	0.63 ± 0.06 | 0.76 ± 0.10	1.0 ± 0.02 | 1.2 ± 0.27

[a]$MIC_{50/90}$: compound concentration leading to 50/90% of growth inhibition, determined by the INT assay following an absorbance reading at 470 nm. Values are the mean values of three independent assays performed in triplicate. VAN, vancomycin; ref., reference drugs. See Supporting Information Table S1 for the resistance profile of the *S. aureus* clinical isolates.[32]

https://doi.org/10.1021/acsinfecdis.6c00165
ACS Infect. Dis. XXXX, XXX, XXX−XXX

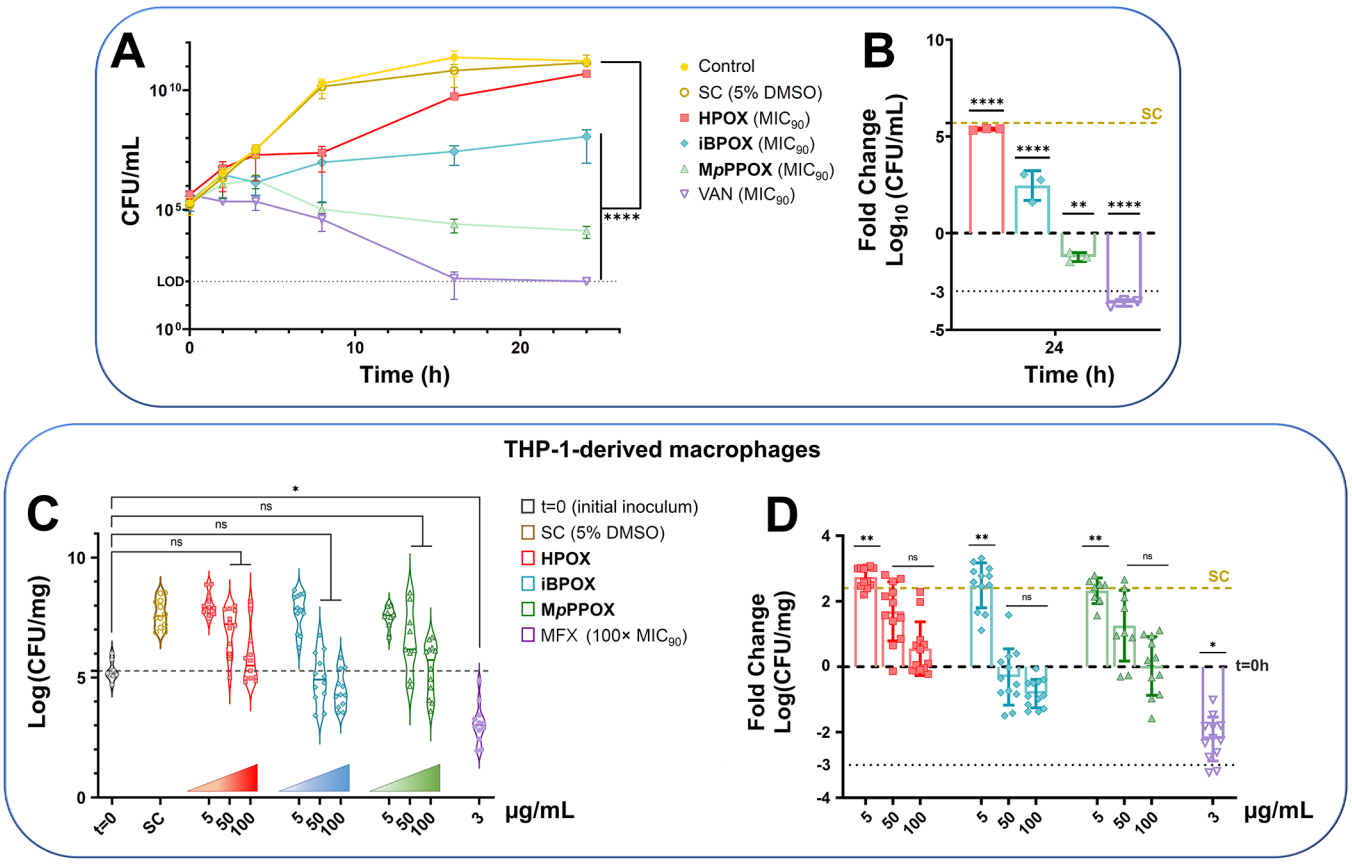

Figure 2. Antibacterial activity of **HPOX**, **iBPOX**, and **MpPPOX** against planktonic and intracellular *S. aureus* ATCC 25923.(A) Time-dependent killing activity curves of the **OX** against *S. aureus* ATCC 25923 planktonic growth. Bacteria (~5×10^5 CFU/mL initial bacterial load) were incubated with each **OX** or vancomycin (VAN) at its respective MIC_{90} concentration. Results are expressed as the mean values ± SD of the number of CFU/mL as a function of time ($n = 3$). (B) Fold change in the logarithm of the number of CFU/mL at 24h versus initial inoculum at $t = 0$. The control conditions were bacteria alone in MHII medium and SC (solvent control), i.e., MHII medium +5% DMSO. The *p*-values are indicative of significant variation in *S. aureus* burden from initial inoculum at $t = 0$. Results are expressed as mean values ± SD of three biologically independent experiments. (C) Intracellular activity of **HPOX**, **iBPOX**, and **MpPPOX** as compared to moxifloxacin (MFX). The activity of selected **OXs** on intracellular *S. aureus* ATCC 25923 was assessed in human THP-1-derived macrophages. Cells were infected at a multiplicity of infection (MOI) of 4 with opsonized *S. aureus* and treated with various concentrations of each inhibitor or MFX for 24 h. Then, surviving bacteria were enumerated by plating serial dilutions of THP-1 lysates. DMSO-treated infected macrophages (SC) represent 100% of bacterial viability. Results are shown as the logarithm of the number of CFU per milligram of proteins (i.e., Log(CFU/mg)) collected from THP-1-derived macrophages after 24 h incubation postphagocytosis, compared to that obtained with the initial postphagocytosis inoculum ($t = 0$). (D) Fold change in the Log(CFU/mg) after 24 h incubation postphagocytosis versus the initial inoculum ($t = 0$). Statistical significance was assessed by Dunnett's multiple comparisons test (one-way ANOVA) using Prism 8.0 (GraphPad, Inc.). The *p*-values were determined between the initial inoculum at $t = 0$ and each condition: ns, not significant (*p*-value >0.05); * *p*-value <0.05. Results are from $n = 3$ biologically independent experiments.

against intracellular *S. aureus* ATCC 25923 inside human THP-1-derived macrophages. Then, THP-1-derived macrophages were infected with *S. aureus* at a multiplicity of infection (MOI) of 4 and incubated for 24 h with each **OX** at final concentrations of 5, 50, and 100 µg/mL that were previously established as noncytotoxic to the cells (Figure 2C,D and Figure S2). To avoid growth of extracellular bacteria, cells were extensively washed and treated with gentamicin (6.25 µg/mL; 50 × MIC_{90}) before incubation with the **OX** analogues. Moxifloxacin (MFX; 3 µg/mL = 100 × MIC_{90}) was used as a positive control for this intracellular killing assay. In each case, the bacterial load was evaluated by CFU counts normalized per milligram of THP-1 cell protein.[36]

First, in the absence of antibiotic or **OXs**, active replication of *S. aureus* ATCC 25923 inside THP-1-derived macrophages was observed. This resulted in an increase of +2.39 Log(CFU/mg) in the bacterial load of the growth control (SC, solvent control). The same replication pattern also occurred at low concentrations of **OXs** (5 µg/mL). However, at 50 and 100 µg/mL, the three **OXs** were able to prevent intracellular bacterial replication, with no statistically significant differences in the bacterial burden at 24 h compared to the initial inoculum ($t = 0$). Notably, 24 h treatment with **iBPOX** resulted in a clear, albeit nonsignificant, reduction in the initial *S. aureus* bacterial load of −0.313 and −0.822 Log(CFU/mg), at 50 and 100 µg/mL, respectively; two concentrations fairly close to its MIC_{90} (65.3 µg/mL).

It is not a new finding that extracellular MIC values do not accurately reflect the potential activity of compounds against intracellular bacteria. Indeed, with regard to *S. aureus*, the intracellular activity of most antibiotics was systematically weaker than their extracellular activity.[36,37] These discrepancies may indeed stem from several factors, including host-cell penetration, accumulation, delivery to the intracellular bacteria, accessibility to their bacterial target enzymes, and compound activity at the acidic phagolysosomal pH (pH ≤ 5.5) of macrophages. Here, both **iBPOX** and **MpPPOX** demonstrated

https://doi.org/10.1021/acsinfecdis.6c00165
ACS Infect. Dis. XXXX, XXX, XXX−XXX

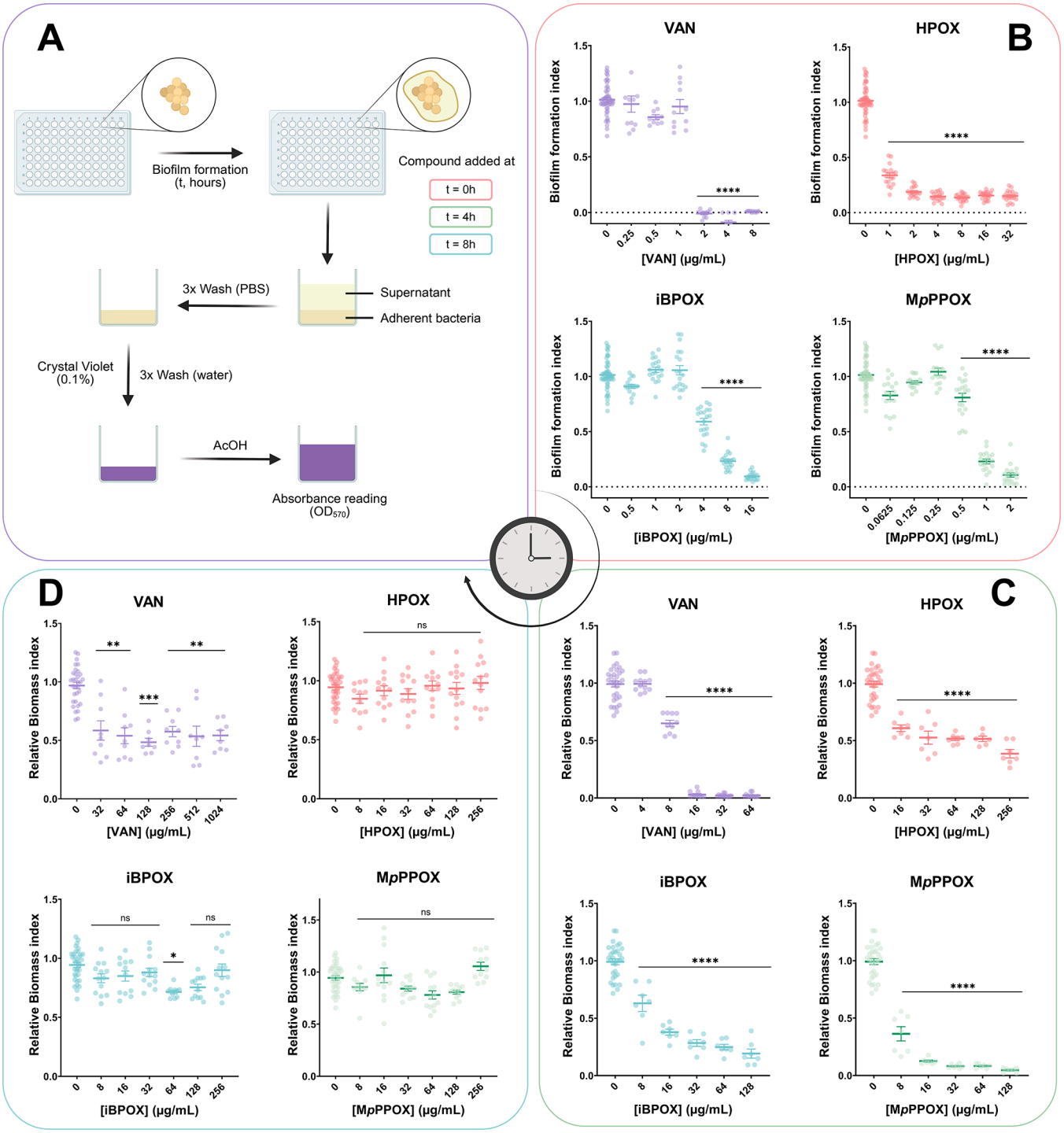

Figure 3. Action of **HPOX**, **iBPOX**, **and MpPPOX** on biofilms of*S. aureus* ATCC 25923.(A) Schematic workflow of biofilm quantification. (B) Relative *S. aureus* biofilm formation index after 6 h of incubation with increasing concentration of the **OXs**. (C) Relative *S. aureus* biofilm formation index after 4 h of growth followed by 8 h of treatment with increasing concentration of the **OXs**. (D) Relative *S. aureus* biofilm formation index after 8 h of growth followed by 16 h of treatment with increasing concentration of the **OXs**. The growth control was the bacteria alone in tryptic soy broth (TSB) medium. Vancomycin (VAN) was used as a positive control. Statistical significance between the growth control and each concentration was assessed by Dunnett's multiple comparisons test (one-way ANOVA) using Prism 8.0 (GraphPad, Inc.). The *p*-value is evaluated between the growth control (0 μg/mL of compound) and each condition: ns, not significant (*p*-value >0.05); *p-value <0.05; **p-value <0.01; ***p-value <0.001; ****p-value <0.0001. Results are from $n = 5$ biologically independent experiments.

enhanced antibacterial activity of 2.1- (MIC_{90} = 30.5 ± 7.8 μg/mL) and 3.1-fold (MIC_{90} = 1.9 ± 0.13 μg/mL), respectively, against planktonic *S. aureus* at acidic pH 5.5 but not **HPOX** (MIC_{90} > 128 μg/mL). This behavior is consistent with the respective observed intracellular antibacterial activity

OXs Prevent the Initial Formation of *S. aureus* Biofilm and Can Potentiate the Antibiofilm Activity of Reference Drugs

Besides intracellular infection and dissemination, the primary cause of the chronicity of *S. aureus* infections is its ability to form biofilms. The physicochemical protection offered by these

https://doi.org/10.1021/acsinfecdis.6c00165
ACS Infect. Dis. XXXX, XXX, XXX−XXX

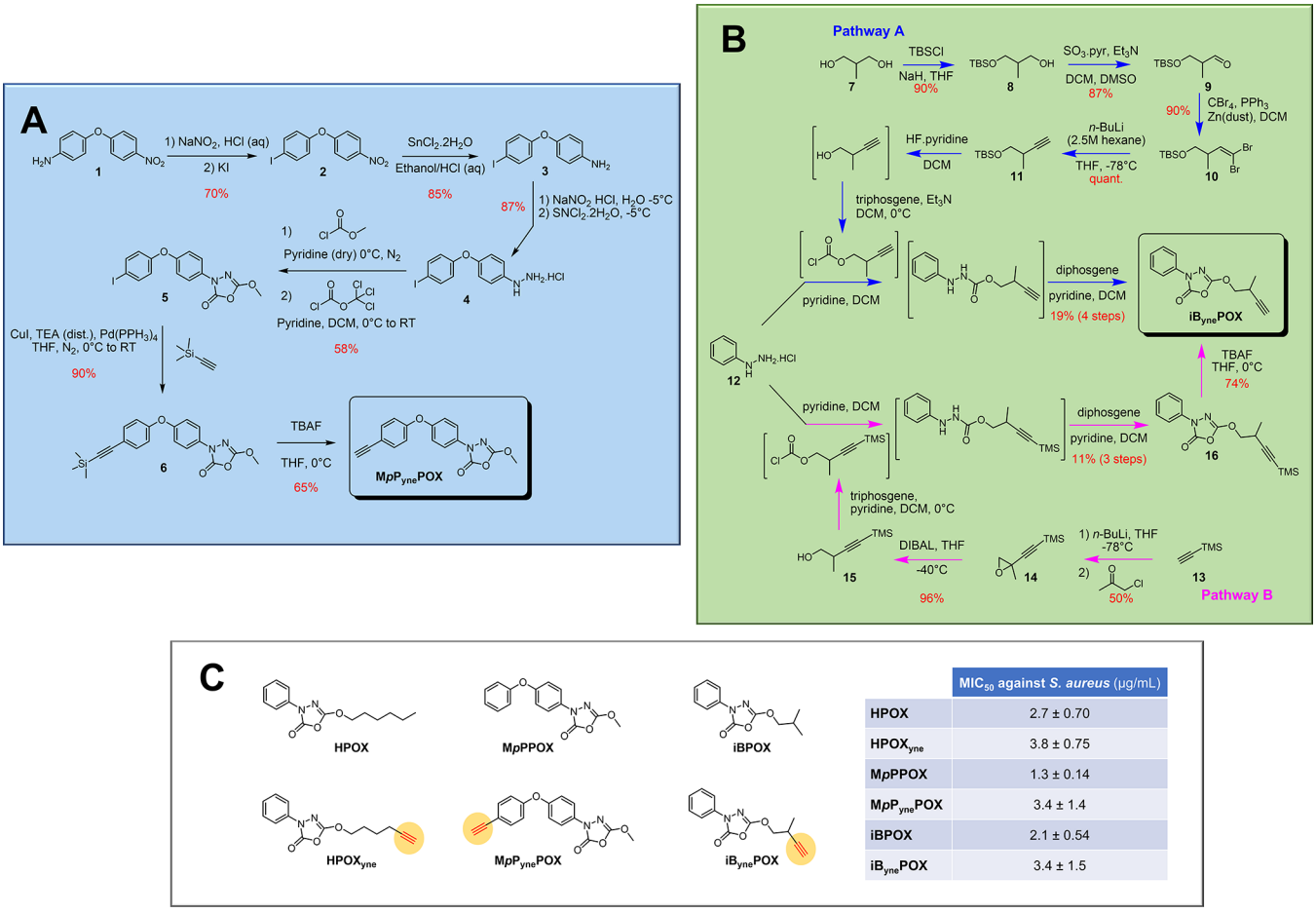

	MIC$_{50}$ against *S. aureus* (μg/mL)
HPOX	2.7 ± 0.70
HPOX$_{yne}$	3.8 ± 0.75
M*p*PPOX	1.3 ± 0.14
M*p*P$_{yne}$POX	3.4 ± 1.4
iBPOX	2.1 ± 0.54
iB$_{yne}$POX	3.4 ± 1.5

Figure 4. Synthesis and antibacterial activity of click-ready **OX$_{yne}$** probes. (A, B) Synthesis of the alkyne derivatives of (A) **M*p*PPOX** bearing an alkyne group on the phenoxyphenyl moiety, i.e., **M*p*P$_{yne}$POX** and (B) **iBPOX** bearing an alkyne group on the isobutyl group, i.e., **iB$_{yne}$POX**. (C) Chemical structure of the thee **OX$_{yne}$** ABPs used in this study, as well as their respective parent molecules. The inset table shows the MIC$_{50}$ values of the three **OX$_{yne}$** against planktonic *S. aureus*, as determined by the INT assay. Results are from $n = 3$ independent assays performed in triplicate.

structures, coupled with a metabolic switch, makes biofilm-embedded bacteria a major therapeutic challenge. In this context, we evaluated the capacity of the three **OXs** to prevent biofilm formation and/or disrupt already formed biofilms, with the aim to determine their minimal biofilm inhibitory concentration (MBIC) and minimal biofilm eradication concentration (MBEC), respectively.[38]

We first evaluate the ability of the three **OXs** to prevent the attachment of *S. aureus* biofilm (Figure 3A,B). Both **M*p*PPOX** and **iBPOX** prevented *S. aureus* biofilm adhesion and formation at sub-MIC$_{90}$ concentrations as low as 0.5 and 4 μg/mL (i.e., 0.0625 × MIC$_{90}$), respectively. Their corresponding MBIC were determined to be 16.3 μg/mL (**iBPOX**) and 1.5 μg/mL (**M*p*PPOX**), thereby corresponding to 0.25 × MIC$_{90}$ (Figure 3B). Remarkably, **HPOX**, which was inactive against planktonic bacteria (MIC$_{90}$ > 128 μg/mL), significantly inhibits biofilm formation at concentrations down to 1 μg/mL, with a calculated MBIC of ∼8 μg/mL.

The maturation time of biofilms significantly impacts the efficacy of antibiotics. The more mature a biofilm is, the less effective the antibiotics will be, including vancomycin. On a 4h-preformed biofilm, **HPOX** and **iBPOX** still disrupted at least 50% of the biomass at concentrations of 32 and 16 μg/mL, respectively. However, only **M*p*PPOX** achieved an MBEC of 16 μg/mL (∼2.7 × MIC$_{90}$) comparable to that of vancomycin (MBEC ∼ 16 μg/mL ⇔ 0.7 × MIC$_{90}$, Figure 3C). After 8 h of maturation, no MBEC was determined for the tested compounds, with even vancomycin barely reaching 50% biofilm disruption at concentrations ≥128 μg/mL (Figure 3D).

It is not surprising that antibacterial compounds lose their efficiency (or part of it) when used against biofilms. These multicellular structures are indeed composed of bacteria embedded in an extracellular polymeric substance (EPS). This EPS physically protects the bacteria against environmental and chemical stresses and creates a unique chemical and enzymatic microenvironment, which contributes to reduce drug's efficacy, consequently increasing antimicrobial tolerance.[7,8]

Indeed, both bacteriostatic (e.g., linezolid) and bactericidal (e.g., gentamicin) antibiotics were inactive against an 8 h preformed *S. aureus* biofilm up to 1024 μg/mL (Figure S3A). On the other hand, rifampicin, another bactericidal drug, showed only a low 34% reduction in the relative biomass index at concentrations ≥ 128 μg/mL (Figure S3A). Such differences in activity for bactericidal antibiotics still remain poorly understood. Some studies have shown that, although both vancomycin and rifampicin can diffuse through an *S. epidermidis* biofilm, this diffusion is insufficient for normal bactericidal action.[39,40] A more recent study hypothesized that the slow passive diffusion of drugs through biofilm would enable bacteria to adapt to higher concentrations of antibiotics.[41] This issue might explain why antibiotics are less efficient against thicker and more mature biofilms.

https://doi.org/10.1021/acsinfecdis.6c00165
ACS Infect. Dis. XXXX, XXX, XXX−XXX

In an effort to take advantage of the **HPOX**-specific activity on biofilm adherence/formation, we evaluated its ability to potentiate the antibiofilm activity of vancomycin, rifampicin, and linezolid on premature biofilms. We thus preincubated *S. aureus* with various concentrations of **HPOX** for 8 h, followed by 16 h of treatment with increasing concentrations of each antibiotic. As expected, preincubation with **HPOX** led to a significant potentiation of all three antibiotics (Figure S3B). Indeed, pretreatment with 16 μg/mL **HPOX** prior to the addition of vancomycin resulted in the inhibition of 72% of biofilm formation (i.e., relative biomass index of 28%) at a low antibiotic concentration of 16 μg/mL. Remarkably, following incubation with 8 μg/mL of **HPOX**, 8 μg/mL of rifampicin was as effective as 128 μg/mL of the drug alone. Ultimately, preincubating *S. aureus* with 8 μg/mL of **HPOX** also enabled the initially ineffective linezolid to achieve 53% inhibition of biofilm at a concentration as low as 16 μg/mL. Based on the observed effects of **HPOX** on initial biofilm formation alone, we can hypothesize that its potentiating effect may be due to reduced bacterial adhesion. As a direct consequence, the resulting planktonic bacteria are less able to protect themselves within the EPS matrix and remain more susceptible to antibiotic treatment.

Overall, our results revealed that **M*p*PPOX** is the only compound tested that displays bactericidal activity similar to vancomycin against both planktonic culture and a 4 h-preformed biofilm of *S. aureus*. On the other side, **HPOX** was identified as a potent antiadhesive agent that impairs *S. aureus* biofilm adhesion/formation and significantly potentiates otherwise ineffective or poorly active drugs. Finally, **iBPOX** exhibited intermediate activity, acting as a bacteriostatic agent against both the planktonic and biofilm forms of *S. aureus*, with the added ability to block intracellular replication. These three molecules act via the same mechanism of action by binding to and inhibiting (Ser/Cys)-based enzymes. They also display close calculated LogP values of 3.69 (**iBPOX**), 4.01 (**M*p*PPOX**), and 4.54 (**HPOX**) at pH 7.4 (using Marvin Suite − ChemAxon), which is indicative of their lipophilic nature. These properties therefore suggest the existence of specific targets that lead to bacterial clearance (**M*p*PPOX**) or play a crucial role in biofilm attachment (**HPOX**).

Synthesis and Antibacterial Activity of OX_{yne} Click-Ready Activity-Based Probes

To confirm this latter hypothesis, click-ready $\mathbf{OX_{yne}}$ activity-based probes (ABPs) of **iBPOX**, **M*p*PPOX**, and **HPOX**, bearing a terminal alkyne function were synthesized (Figure 4), and used in a click-chemistry activity-based protein profiling (CC-ABPP) approach[19,22,26,27,42,43] to capture and identify their respective *S. aureus* target enzymes.

The synthesis of the $\mathbf{OX_{yne}}$ probe of **M*p*PPOX** bearing an alkyne group on the phenoxy moiety (**M*p*P$_{yne}$POX**, Figure 4A) was achieved through a late-stage introduction of the ethynyl group. The strategy began with the preparation of iodinated phenoxy precursor **2** via a Sandmeyer reaction performed on 4-(*p*-nitrophenoxy)aniline **1**, followed by the reduction of the nitro group to afford the corresponding aniline **3**. This intermediate was converted to the hydrazine **4**. The oxadiazolone core was then constructed in two one-pot successive steps using methyl chloroformate and diphosgene.[24] The resulting iodinated oxadiazolone **5** was involved in a Sonogashira coupling[44] with trimethylsilylacetylene to afford compound **6**. Finally, desilylation of **6** using a catalytic amount of TBAF provided the desired compound **M*p*P$_{yne}$POX** in 17% overall yield (Figure 4A).

The synthesis of the alkyne analogue of **iBPOX** (**iB$_{yne}$POX**, Figure 4B) was more complex because of the position of the alkyne on the isobutyl moiety of the **OX** structure, which required a propargylic alcohol precursor that was not commercially available. This synthesis was envisaged to occur through two different pathways. Pathway A started from the 2-methyl-1,3-propandiol **7**, selectively monoprotected by TBS groups. The free alcohol function of **8** was oxidized to the corresponding aldehyde **9** to perform the one-carbon homologation using the Corey−Fuchs process[45] in two steps.[46] CBr_4 equivalents were reduced to 2 equiv to ensure adequate workup and purification during the dibromo **10** synthesis. The following halogen-metal exchange/elimination steps were realized in the presence of *n*-BuLi and afforded the protected alkyne **11** in quantitative yield. Deprotection of the silylated protecting groups was performed by using HF in pyridine. Despite efficient conversion of the reaction, the resulting alcohol was impossible to purify because of its degradation during purification on column chromatography. The reaction was then performed in DCM and carefully evaporated to engage the crude volatile alcohol derivative in the preparation of the chloroformate. The formation of the desired oxadiazolone **iB$_{yne}$POX** was finally achieved using classical one-pot methodology from the crude chloroformate and commercial phenylhydrazine hydrochloride **12**.[24] Despite an acceptable global yield of 13.4% over eight steps, Pathway A suffers from drawbacks mainly related to the purification of the dibromo derivative **10** and the impossible purification of the propargylic alcohol that imposes a one-pot reaction of four steps, leading to a challenging final purification. Pathway B has two fewer steps than Pathway A. Starting from trimethylsilyl acetylene **13**, elongation of the carbon chain was performed using chloroacetone in the presence of *n*-BuLi, leading to the epoxide **14**.[47] DIBAL-H reduction allowed ring opening of the epoxide and afforded the alcohol **15**. Then, the classical cyclization-oxadiazolone ring formation was conducted using the corresponding chloroformate of alcohol **15** and phenylhydrazine hydrochloride **12**. To perform the final TMS deprotection of **16**, basic conditions using K_2CO_3 in MeOH were not compatible with the oxadiazolone ring stability. To overcome this issue, catalytic amounts of TBAF were used to avoid ring opening, thereby affording the desired **iB$_{yne}$POX** in good 74% yield. Despite a lower global yield of 4% (over six steps), Pathway B still represents an interesting alternative since it allows an overall improvement of the purifications as well as technically easier steps.

Finally, the $\mathbf{HPOX_{yne}}$ probe was synthesized as described previously.[48]

As a prerequisite, the antimicrobial activities of the three $\mathbf{OX_{yne}}$ probes were assessed against *S. aureus* ATCC 25923 and compared to those of the parent molecules **HPOX**, **M*p*PPOX**, and **iBPOX**. As depicted in Figure 4C, comparable MIC_{50} values were obtained for each **OX**/$\mathbf{OX_{yne}}$ couple: **HPOX**/$\mathbf{HPOX_{yne}}$ (2.7/3.8 μg/mL), **M*p*PPOX**/**M*p*P$_{yne}$POX** (1.3/3.4 μg/mL), and **iBPOX**/**iB$_{yne}$POX** (2.1/3.4 μg/mL). Given these results, $\mathbf{HPOX_{yne}}$, **M*p*P$_{yne}$POX**, and **iB$_{yne}$POX** were used as affinity-based probes in a CC-ABPP strategy. This method, thoroughly described in previous works, has already proven to be a powerful tool to gain insight into the proteins targeted by our **OX** molecules.[22,43,48]

https://doi.org/10.1021/acsinfecdis.6c00165
ACS Infect. Dis. XXXX, XXX, XXX−XXX

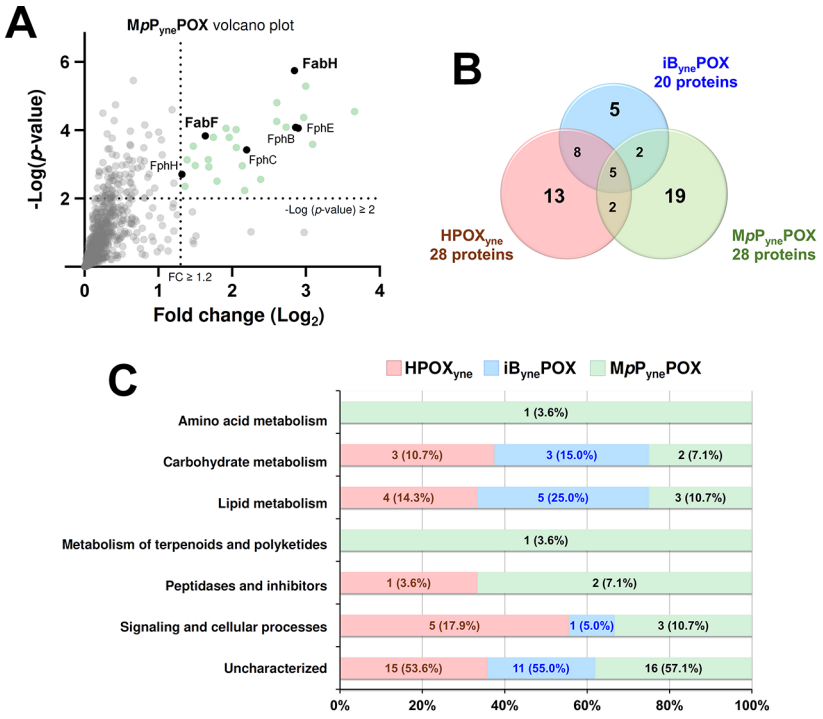

Figure 5. Proteomics analysis of click-chemistry activity-based profiling (CC-ABPP) on *S. aureus* ATCC 25923 culture. (A) Volcano plot of the proteomics analysis of **MpP$_{yne}$POX** in *S. aureus* ATCC 25923 culture showing the significance of two-sample *t*-test (−log(*p*-value)) versus fold change (Log_2(LFQ normalized intensity in **MpP$_{yne}$POX** versus nonspecific conditions)) on the *y* and *x* axes, respectively. The dashed lines indicate the threshold of *p*-value <0.01 and a fold change (Log_2) ≥ 1.2. (B) Venn diagram showing the total number of proteins differentially captured with each **OX$_{yne}$** probe at a *p*-value ≤ 0.01 and a fold change (Log_2) ≥ 1.2. (C) Repartition of functional categories of *S. aureus* ATCC 25923 proteins identified with **HPOX$_{yne}$**, **iB$_{yne}$POX**, or **MpP$_{yne}$POX** according to the functional classification system of the KEGG database. The numbers correspond to the total number of proteins identified in each category, with the corresponding percentage in parentheses related to either the 28, 20, or 28 proteins identified with **HPOX$_{yne}$**, **iB$_{yne}$POX**, or **MpP$_{yne}$POX**, respectively. Proteins with no annotation are denoted as uncharacterized proteins. See also Supporting Information Tables S2−S4. Results are from *n* = 3 biologically independent experiments.

MpPPOX- and HPOX-Specific Target Proteins in *S. aureus* Correlate with Their Respective Observed Compound-Specific Antibacterial Activities

S. aureus cells in the mid log growth phase were incubated with each **OXyne** probe or dimethyl sulfoxide (DMSO). The cells were lysed and subjected to a biorthogonal covalent click-chemistry reaction using a desthiobiotin-PEG$_3$-N$_3$ reporter to enable affinity enrichment. Following on-bead tryptic digestion, the resulting peptides were analyzed by liquid chromatography-tandem mass spectrometry (LC-MS/MS) and quantified by label-free quantitative analysis.

After applying threshold values of *p*-value ≤ 0.01 (i.e., -Log(*p*-value) ≥ 2) and fold change (Log_2) ≥ 1.2 on the comparative proteomic analysis between the control DMSO-treated sample and the **OX$_{yne}$**-treated samples (Figure 5A), 28, 20, and 28 protein candidates were identified with **HPOX$_{yne}$**, **iB$_{yne}$POX**, and **MpP$_{yne}$POX**, respectively (Figure 5B, Table 3, and Tables S2−S4). Several different functional categories have been identified, illustrating the ubiquity of (Ser/Cys)-based enzymes, with however a large majority of either poorly annotated or uncharacterized proteins (Figure 5C).

Of the annotated targets, proteins involved in carbohydrate and lipid metabolisms, as well as in cellular processes, are the most abundant and are equally captured by all three probes. In agreement with previous CC-ABPP works with *S. aureus* using oxadiazolone-core probes closely related to the **MpPPOX** chemical structure,[19,26,27] the fluorophosphonate-binding hydrolases FphB, FphC, FphE, and FphH were identified only with **MpP$_{yne}$POX** (Figure 5A and Table 3). Of interest, four essential proteins were also identified, including, the 3-oxoacyl-[acyl-carrier-protein] synthase 2 (FabF, SAOUHSC_00921) and the *β*-ketoacyl-[acyl-carrier-protein] synthase III (FabH, SAOUHSC_00920), two well-known therapeutic targets belonging to the FAS II pathway.[49,50] While these two targets were captured by all three probes, different affinities were however observed (Tables S2−S4). Indeed, the highest enrichment scores for FabF and FabH were reached with **MpP$_{yne}$POX** (fold change (Log_2) values of 1.63 and 2.84, respectively), followed by **iB$_{yne}$POX** (fold change (Log_2) values of 1.52 and 1.53, respectively), and finally **HPOX$_{yne}$** (fold change (Log_2) values of 1.23 and 1.09, respectively). Notably, the fold change value of 1.09 for FabH with the latter **HPOX$_{yne}$** probe was below the fixed threshold of 1.2.

Regarding this latter compound, most of its target enzymes have been reported as participating in *S. aureus* virulence and biofilm formation. These included the leucocidin-like protein 2 (SAOUHSC_02243) and the fibrinogen-binding protein (SAOUHSC_01110) that play key role in biofilm formation;[51−54] the gamma-hemolysin toxins Hlg (SAOUHSC_02708), HlgC (SAOUHSC_02709), and HlgB (SAOUHSC_02710), which are important virulence factors involved in biofilm immune evasion;[51] Lipase1 (SAL1, SAOUHSC_03006) and Lipase2 (SAL2, SAOUHSC_00300), two serine hydrolyses active under biofilm forming conditions,[55] and also captured by **iB$_{yne}$POX**; and two secreted exotoxin virulence factors, the *β*-hemolysin Hlb (SAOUHSC_02240) and Staphopain B (SAOUHSC_00987).[56] Finally, the 5′-nucleotidase, lipoprotein e(P4) family (SAOUHSC_00284)

https://doi.org/10.1021/acsinfecdis.6c00165
ACS Infect. Dis. XXXX, XXX, XXX−XXX

Table 3. *S. aureus* ATCC 25923 Target Proteins Identified by CC-ABPP with the three OX_{yne} Affinity-Based Probes

$HPOX_{yne}$	$iB_{yne}POX$	$MpP_{yne}POX$	pathways	gene names	essentiality[a]	protein names
		+	amino acid metabolism	SAOUHSC_02259	nonessential	omega-amidase
+	+	+	carbohydrate metabolism	SAOUHSC_00132	nonessential	putative aldehyde dehydrogenase, AldA
+	+		carbohydrate metabolism	SAOUHSC_02352	nonessential	UDP-*N*-acetylglucosamine 2-epimerase
+	+	+	carbohydrate metabolism	SAOUHSC_02363	nonessential	putative aldehyde dehydrogenase
+	+	+	lipid metabolism	SAOUHSC_00195	nonessential	probable acetyl-CoA acyltransferase
+	+		lipid metabolism	SAOUHSC_00300	nonessential	lipase 2, SAL2
		+	lipid metabolism	SAOUHSC_00558	nonessential	putative acetyl-CoA C-acetyltransferase, VraB
+			lipid metabolism	SAOUHSC_00728	essential	lipoteichoic acid synthase, LtaS
	+	+	lipid metabolism	SAOUHSC_00920	essential	*β*-ketoacyl-[acyl-carrier-protein] synthase III, FabH
+	+	+	lipid metabolism	SAOUHSC_00921	essential	3-oxoacyl-[acyl-carrier-protein] synthase 2, FabF
+	+		lipid metabolism	SAOUHSC_03006	nonessential	lipase 1, SAL1
		+	metabolism of terpenoids and polyketides	SAOUHSC_02142	nonessential	4,4′-diaponeurosporen-aldehyde dehydrogenase
		+	peptidases and inhibitors	SAOUHSC_00247	nonessential	penicillin V amidase
+			peptidases and inhibitors	SAOUHSC_00987	nonessential	staphopain B, SspB
		+	peptidases and inhibitors	SAOUHSC_02834	nonessential	sortase A
+	+		signaling and cellular processes	SAOUHSC_00229	nonessential	iron−sulfur cluster repair protein, ScdA
+			signaling and cellular processes	SAOUHSC_00667	nonessential	putative hemin import ATP-binding protein, HrtA
+			signaling and cellular processes	SAOUHSC_02240	nonessential	beta-hemolysin, Hlb
+		+	signaling and cellular processes	SAOUHSC_02241	nonessential	uncharacterized leukocidin-like protein 1
		+	signaling and cellular processes	SAOUHSC_02261	nonessential	accessory gene regulator protein B
+			signaling and cellular processes	SAOUHSC_02708	nonessential	gamma-hemolysin h-gamma-II subunit
+			signaling and cellular processes	SAOUHSC_02709	nonessential	gamma-hemolysin component C, HlgC
+			signaling and cellular processes	SAOUHSC_02710	nonessential	gamma-hemolysin component B, HlgB
		+	uncharacterized protein	SAOUHSC_00237	nonessential	putative methyltransferase
+			uncharacterized protein	SAOUHSC_00284	nonessential	5′-nucleotidase, lipoprotein e(P4) family
+	+	+	uncharacterized protein	SAOUHSC_00301	nonessential	uncharacterized protein
	+		uncharacterized protein	SAOUHSC_00362	nonessential	NDxxF motif lipoprotein
		+	uncharacterized protein	SAOUHSC_00417	nonessential	putative Serine aminopeptidase
	+		uncharacterized protein	SAOUHSC_00604	nonessential	FMN-dependent NADPH-azoreductase
+			uncharacterized protein	SAOUHSC_00774	nonessential	uncharacterized protein
		+	uncharacterized protein	SAOUHSC_00802	nonessential	putative carboxylesterase, FphH
+			uncharacterized protein	SAOUHSC_00845	nonessential	uncharacterized protein
+			uncharacterized protein	SAOUHSC_01061	nonessential	uncharacterized protein
+			uncharacterized protein	SAOUHSC_01110	nonessential	fibrinogen-binding protein
		+	uncharacterized protein	SAOUHSC_01279	nonessential	putative hydrolase, FphC
	+	+	uncharacterized protein	SAOUHSC_01282	nonessential	glutathione peroxidase
+	+		uncharacterized protein	SAOUHSC_01627	essential	hypothetical lipoprotein
+	+		uncharacterized protein	SAOUHSC_01854	nonessential	uncharacterized protein
		+	uncharacterized protein	SAOUHSC_02145	nonessential	phage protein
+			uncharacterized protein	SAOUHSC_02243	nonessential	uncharacterized leukocidin-like protein 2
	+		uncharacterized protein	SAOUHSC_02355	nonessential	uncharacterized protein
		+	uncharacterized protein	SAOUHSC_02376	nonessential	DoxX family membrane protein
		+	uncharacterized protein	SAOUHSC_02382	nonessential	uncharacterized protein
+	+		uncharacterized protein	SAOUHSC_02637	nonessential	uncharacterized protein
+		+	uncharacterized protein	SAOUHSC_02645	nonessential	uncharacterized protein
		+	uncharacterized protein	SAOUHSC_02706	nonessential	immunoglobulin-binding protein, Sbi
	+		uncharacterized protein	SAOUHSC_02759	nonessential	uncharacterized protein
		+	uncharacterized protein	SAOUHSC_02844	nonessential	putative alpha/beta hydrolase, FphB
		+	uncharacterized protein	SAOUHSC_02900	nonessential	uncharacterized hydrolase, FphE
		+	uncharacterized protein	SAOUHSC_02915	nonessential	putative Xaa-Pro dipeptidyl-peptidase
+	+		uncharacterized protein	SAOUHSC_02962	nonessential	*S*-formylglutathione hydrolase
	+		uncharacterized protein	SAOUHSC_02972	nonessential	immunodominant staphylococcal antigen B
		+	uncharacterized protein	SAOUHSC_02994	nonessential	DoxX family membrane protein
		+	uncharacterized protein	SAOUHSC_03034	nonessential	arylamine *N*-acetyltransferase

[a]The essentiality of each *S. aureus* ATCC 25923 gene is checked using Table S1 from Chaudhuri et al.[60]

https://doi.org/10.1021/acsinfecdis.6c00165
ACS Infect. Dis. XXXX, XXX, XXX−XXX

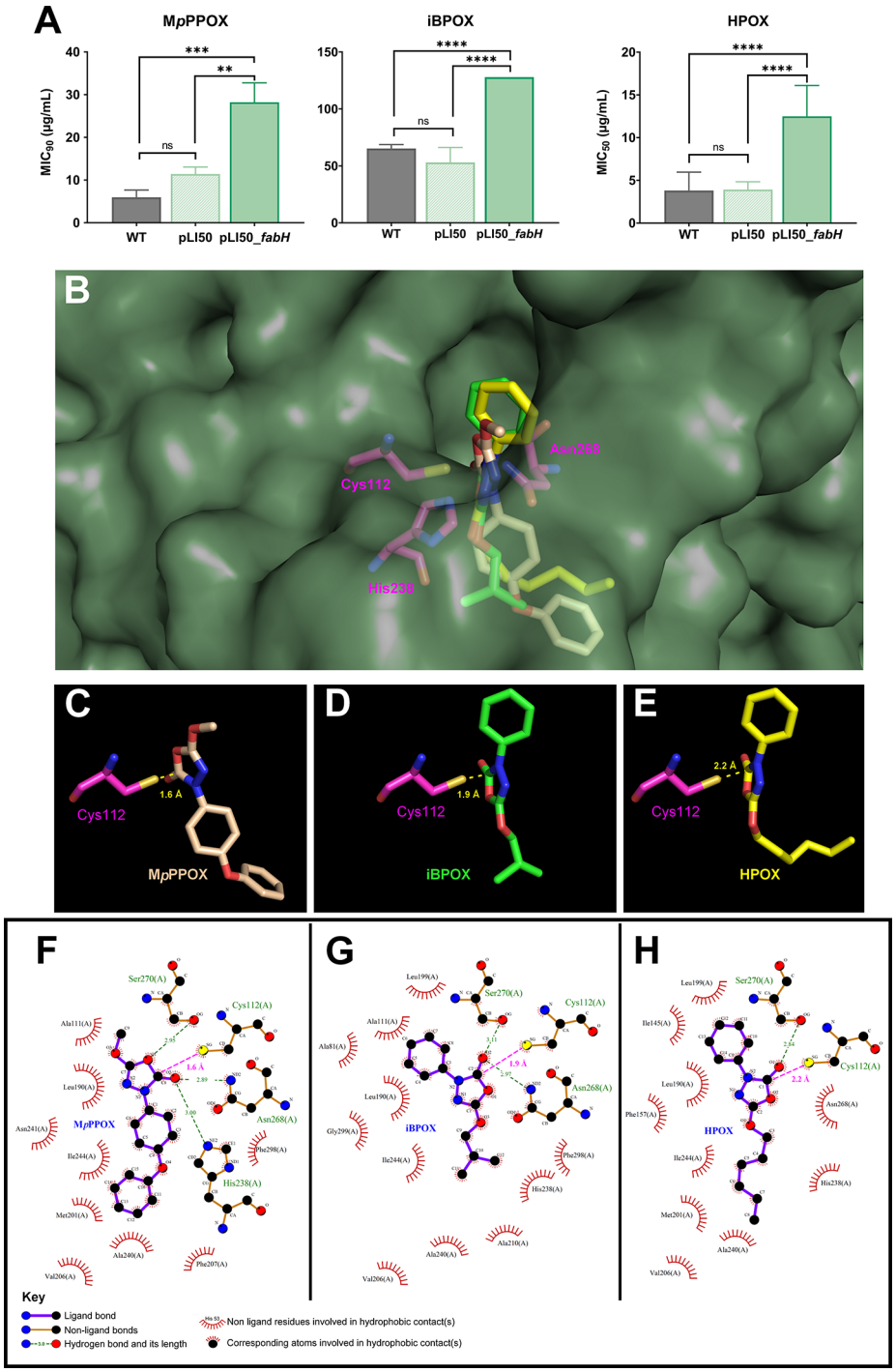

Figure 6. Functional validation of FabH as a vulnerable target of ***Mp*PPOX**. (A) MICs of ***Mp*PPOX**, **iBPOX**, and **HPOX** against *S. aureus*-pLI50_*fabH* overexpression strain as compared to WT strain and pLI50_empty vector. ns, not significant (p-value >0.05); **p-value <0.01; ***p-value <0.001. Results are from $n = 3$ biologically independent experiments. (B) In silico molecular docking of ***Mp*PPOX** (wheat color), **iBPOX** (green color), and **HPOX** (yellow color) into the crystallographic structure of *Sa*FabH in a surface representation. The Cys^{112}-His^{238}-Asn^{268} catalytic residues of *Sa*FabH are in magenta stick representation. (C–E) Top-scoring docking position of (C) ***Mp*PPOX**, (D) **iBPOX**, and (E) **HPOX** in the vicinity of Cys^{112}. Each inhibitor is in stick representation with the atom color code: oxygen, red; nitrogen, blue; carbon, wheat, green, or yellow. Structures were drawn with PyMOL Molecular Graphics System (Schrödinger, LLC) using the PDB file 1ZOW.[63] (F–H) Ligplot$^+$ analyses results: 2D representation of hydrogen-bonds and hydrophobic interactions of (F) ***Mp*PPOX**, (G) **iBPOX**, and (F) **HPOX** inside *Sa*FabH active site.

and the essential lipoteichoic acid synthase LtaS (SAOUHSC_00728) implicated in the membrane modeling,[57,58] were also identified. Therefore, $\mathbf{HPOX}_{\mathbf{yne}}$-specific enzymes align with the observed antibiofilm effect of **HPOX**, but also suggest that this **OX** might have potential antivirulence properties as well. However, further mechanistic studies involving knockdown/overexpression mutant strains or inhibition studies on key individual targets will be necessary to fully elucidate the mechanism of **HPOX**-specific antibiofilm activity.

Overall, these results not only corroborate the multitarget nature of the **OXs**, as demonstrated in previous studies on mycobacteria[20,21,23,24] or *S. aureus*,[19,26,27] but they also

https://doi.org/10.1021/acsinfecdis.6c00165
ACS Infect. Dis. XXXX, XXX, XXX−XXX

emphasize the complementary selectivity of the three $\mathbf{OX_{yne}}$ probes, which differ in their chemical structure around the oxadiazolone ring. Although they target similar biological processes, as shown in the functional categorization profile of the captured proteins, these probes indeed act on different enzymes in accordance with their respective antibacterial activity.

FabH Is A Vulnerable Target of M*p*PPOX

FabH, which plays pivotal roles in both initiation and regulation of the fatty acid biosynthesis process,[49,50] has been identified in previous ABPP experiments involving oxadiazolone-core molecules.[23,24] Since a single *fabH* gene has been identified in the genome of *S. aureus*[59] and given its essentiality,[60] this prompted us to hypothesize that this enzyme could be at the core of **M*p*PPOX** bactericidal activity.

We then constructed a 6 × His-tagged FabH overexpression strain in the *S. aureus* ATCC 25923 genetic background. Using a restriction-free cloning approach, *fabH* coding sequence was cloned and overexpressed in *S. aureus* ATCC 25923 using the pLI50 medium-copy plasmid under the control of the native *hpf* promoter (Figure S4A). Successful cloning was checked by PCR (Figure S4B), and protein expression was confirmed by Western Blotting (Figure S4C).

To examine the susceptibility of the *S. aureus*-pLI50_*fabH* overexpression strain, MIC_{90} values of **M*p*PPOX**, **iBPOX**, **HPOX**, vancomycin, and gentamicin were determined and compared to the *S. aureus*-pLI50_empty vector and the parental (WT) strain (Figure 6A and Figure S4D). As expected, no changes were found for vancomycin (MIC_{90} ~0.89−1.48 μg/mL) and gentamicin (MIC_{90} ~0.36−0.47 μg/mL, Figure S4D). With **HPOX** ($MIC_{90} \geq 128$ μg/mL, Figure S4D), a 3.2-fold increase in MIC_{50} (12.5 ± 2.1 μg/mL) was however observed (Figure 6A). Conversely, with **M*p*PPOX**, overexpression of FabH led to a significant 4.7-fold increase in the MIC_{90} value (28.2 ± 4.5 μg/mL) as compared to the WT strain (5.9 ± 1.7 μg/mL; *p*-value <0.001) and a 2.5-fold increase as compared to the *S. aureus*-pLI50_empty vector (11.4 ± 1.6 μg/mL; *p*-value <0.01). Finally, a MIC_{90} > 128 μg/mL (*p*-value <0.001) was achieved with **iBPOX** (Figure 6A).

This slight, but statistically significant, increased resistance level observed with the *S. aureus*-pLI50_*fabH* overexpression strain is consistent with the notion that overexpressing a single potential target enzyme will not result in high levels of resistance in the presence of multitarget agents. Nevertheless, these results also imply that FabH is an effective drug target for **M*p*PPOX**, **iBPOX**, and to a lesser extent **HPOX**.

In order to shed light on the significant discrepancy in antibacterial activity observed between the three **OXs**, in silico molecular docking experiments were conducted, as described previously[43,61,62] using the reported crystal structure of *S. aureus* FabH (*Sa*FabH; PDB: 1ZOW).[63] These experiments aimed to elucidate the potential interactions occurring at the enzyme's active site that drive the binding mode of the two **OXs**. In both cases, the best-scoring position obtained (i.e., lowest energy complex) showed that the three **OXs** would adopt a comparable productive orientation inside the enzyme active site (Figure 6B). With **M*p*PPOX**, the sp^2 carbon atom of the oxadiazolone moiety is 1.6 Å away from the catalytic Cys^{112}, supporting the occurrence of a strong covalent interaction (Figure 6C). Conversely, the carbonyl group of **HPOX** is positioned 2.2 Å farther away from the catalytic Cys^{112} (Figure 6E). Moreover, these two optimal docking poses correlated with distinct predicted binding energy values. Indeed, with a lower and more favorable predicted binding energy, $\Delta E_{MpPPOX} = -8.3$ kcal.mol^{-1}, **M*p*PPOX** is expected to exhibit a stronger affinity for the *Sa*FabH active site than **HPOX** ($\Delta E_{HPOX} = -6.8$ kcal.mol^{-1}).

The key stabilizing residues of *Sa*FabH involved in the molecular interactions with **M*p*PPOX** or **HPOX** within the enzyme active site were further visualized using Ligplot+.[64] In the obtained binding model (Figure 6F), the phenoxyphenyl group of **M*p*PPOX** is stabilized by nine hydrophobic interactions with Ala^{111}, Leu^{190}, Met^{201}, Val^{206}, Phe^{207}, Ala^{240}, Asn^{241}, Ile^{244}, and Phe^{298} and three H-bonding with His^{238}, Asn^{268}, and Ser^{270} residues. Such interactions result in a strong stabilization of the sp^2 carbonyl group near the catalytic Cys^{112}. By contrast, with **HPOX**, the hexyl chain is involved in binding interactions with seven residues (i.e., Phe^{157}, Met^{201}, Val^{206}, His^{238}, Ala^{240}, Ile^{244}, and Asn^{268}), while the phenyl ring positioned at the right entrance to the catalytic cleft is stabilized by long-distance hydrophobic interactions with three residues (i.e., Ile^{145}, Leu^{190}, and Leu^{199}). Finally, the oxadiazolone ring would only be stabilized by one H-bond with the Ser^{270} residue (Figure 6H). Regarding **iBPOX**, the compound behaves exactly as an intermediate between **M*p*PPOX** and **HPOX**: located 1.9 Å from Cys^{112} with a binding energy $\Delta E_{iBPOX} = -7.4$ kcal.mol^{-1} and stabilizing residues similar to **M*p*PPOX** (Figure 6D,G).

Additionally, a high level of concordance was observed between the top-ranked docked pose of **M*p*PPOX** and the crystal structure of the 4-chloro-*N*-((*N*-(cyclopropylmethyl)-formamido)methyl)benzamide (*i.e.*, **OAX**) inhibitor covalently bound to Cys^{112} inside the *Sa*FabH active site (Figure S5).

Together, the differences in the binding modes of the three compounds (Δ*E*, distance from the Cys^{112}, Ligplot^{+} diagram analysis) provide a clear picture of *Sa*FabH inhibition, thereby exemplifying selective enzyme recognition to each **OX**. This might also bring some explanations for the high discrepancy observed in experimental MICs.

CONCLUSIONS

In this study, we investigated the biological effects of various oxadiazolone-core compounds against planktonic, biofilm, and intracellular lifeforms of *S. aureus*. As previously observed in the case of mycobacterial species,[21,23,24] the antibacterial activity against *S. aureus* varied substantially depending on the compound tested, with no real structure−activity tendency. Indeed, while some **OXs** were completely inactive, others showed promise in terms of their antibacterial or antibiofilm activity. This was particularly the case of **HPOX**, **iBPOX**, and **M*p*PPOX**, which showed distinct activities. **HPOX** was inactive against both planktonic and intracellular bacteria but displayed a potent activity against the initial adhesion of *S. aureus* biofilms, even at very low concentrations. On the other hand, **M*p*PPOX** was able to efficiently kill planktonic bacteria and disrupt a 4 h preformed biofilm of *S. aureus*. Finally, **iBPOX** was found to primarily inhibit intracellular replication and demonstrate moderate bacteriostatic activity against both planktonic and biofilm-associated *S. aureus*. Using derived "click-ready" alkyne probes allows for the direct capture of their respective target enzymes in bacterial cultures, confirming their multitarget nature. Of interest, the identified targets were efficiently correlated with the observed antibacterial activity. Among these targets, the essential β-ketoacyl-[acyl-carrier-protein] synthase III, FabH protein, has been confirmed as a vulnerable target of **M*p*PPOX**. Overall, our study emphasized the use of the

https://doi.org/10.1021/acsinfecdis.6c00165
ACS Infect. Dis. XXXX, XXX, XXX−XXX

OX derivatives as an attractive option in the development of novel multitarget inhibitors of pulmonary pathogens, including *S. aureus* but also *M. tuberculosis* or *M. abscessus*, thereby opening new opportunities in the fight against drug-resistant bacteria. These **OXs** could also serve as probes, not only to dissect their molecular bacterial targets, but also to identify by CC-ABPP their bacterial target enzymes inside infected macrophages.

MATERIAL AND METHODS

Chemistry

The oxadiazolone derivatives **iBPOX**, **iBpPPOX**, **HPOX**, **MPOX**, **MpPPOX**, **MmPPOX**, **MemPPOX**, and **HPOX$_{yne}$** were synthesized, as described previously.[24,48] Detailed procedures and full chemical characterization (^{1}H and ^{13}C NMR spectra) of the new **OX** probes (i.e., **MpP$_{yne}$POX** and **iB$_{yne}$POX**) are reported in the Supporting Information. Each **OX** molecule (purity ≥ 95%) was stored at 4 °C as a 10 mM stock solution in dimethyl sulfoxide (DMSO).

Biological Evaluation

All detailed protocols are given in the Supporting Information.

Bacterial Strain and Growth Conditions. The strains used in this study are listed in Supporting Information Table S5. Bacteria were stored at −80 °C in 25% (v/v) glycerol for cryoprotection. Unless otherwise noted, cells were grown aerobically at 37 °C in cation-adjusted Mueller-Hinton (MHII; Sigma-Aldrich, St Quentin-Fallavier, France, #70192) broth.

MIC Determination. The **OXs** were screened against all *S. aureus* strains, and their respective minimum inhibitory concentrations leading to 50% and 90% of bacterial growth inhibition (MIC_{50} and MIC_{90}, respectively) were determined by the *p*-iodonitrophenyltetrazolium violet (INT) colorimetric assay following absorbance reading at 470 nm,[29,30] as previously described.[22]

Time-Kill Assay. A time-kill assay was conducted with **HPOX**, **iBPOX**, and **MpPPOX** (MIC_{90} of >128, 65.3, and 3.82 μg/mL, respectively). The method was similar to that of MIC determination. Control vessel (5% DMSO) and bactericidal control (2 μg/mL VAN) were included. At each time point, 20 μL of each condition was 10-fold diluted in PBS, and two to three dilutions were plated onto MHII agar plates. The plates were incubated at 37 °C overnight for CFU count.

Intracellular Activity Assay: Adapted from Reference .[37] Culture of human THP-1 monocytes was performed in RPMI-1640 medium (Sigma-Aldrich, #R8758) supplemented with 10% heat-inactivated fetal bovine serum (FBS; Invitrogen, #A5670801) ($RPMI^{FBS}$), and the cells were differentiated with 100 ng/mL of PMA (Phorbol 12-Myristate 13-Acetate; Sigma-Aldrich, #P8139) for 24 h. Infection was performed at MOI 4:1, and the intracellular growth of *S. aureus* ATCC 25923 was assessed after a 24 h period of exposure to the **OXs** at 100, 50, and 5 μg/mL. To avoid extracellular bacterial growth, cells were extensively washed and treated with gentamicin (6.25 μg/mL; 50 × MIC_{90}) before **OXs** treatment. Moxifloxacin (MFX; 3 μg/mL; 100 × MIC_{90}) was used as a positive control.

Inhibition of Biofilm Formation. The capacity of **HPOX**, **iBPOX**, and **MpPPOX** to prevent biofilm adhesion was assessed. Briefly, bacteria from an overnight culture in Tryptic Soy Broth (TSB; Sigma-Aldrich, #1.05459) were used to prepare an inoculum of 2 × 10^6 CFU/mL. Then, 100 μL of this inoculum was added to a 96-well microplate to 100 μL of TSB containing 2-fold serial dilutions of each compound and incubated for 6 h at 37 °C. $OD_{600\ nm}$ was measured to evaluate planktonic growth, and the microplate was washed with PBS before staining the remaining biofilm with crystal violet (0.1%, w/v). $OD_{570\ nm}$ measurement allows to evaluate the quantity of adherent bacteria. The results were normalized using the growth control as 100%.

Disruption of Mature Biofilm. The capacity of the **HPOX**, **iBPOX**, and **MpPPOX** to disrupt a mature biofilm and kill bacteria inside the biofilm matrix was further investigated. Briefly, bacteria from an overnight culture in TSB were used to prepare an inoculum of 1 × 10^6 CFU/mL, and 200 μL of this inoculum was added to 96-well flat-bottom microplates with a lid. The microplates were incubated at 37 °C for either 4 or 8 h to allow for biofilm formation. The medium was replaced with fresh media containing 2-fold dilutions of the tested **OXs**. The microplates were left at 37 °C for 8 or 16 h and processed as for biofilm formation.

Activity-Based Protein Profiling: Adapted from References 22 and 43

Capture of *S. aureus* ATCC 25923 Target Proteins from iB$_{yne}$POX-, MpP$_{yne}$POX-, and HPOX$_{yne}$-Treated Culture via Click Chemistry. Fresh mid log phase bacterial suspension in MHII broth was pelleted and resuspended to a final volume of 1 mL at $OD_{600\ nm}$ = 20. The bacterial cells were incubated overnight at 37 °C at 180 rpm with each **OX$_{yne}$** probe (500 μM final concentration), or DMSO (control). Bacteria were washed and resuspended in PBS supplemented with complete Mini EDTA-free protease inhibitors (Roche, Mannheim, Germany) before being lysed by mechanical disruption using a Mini-Beadbeater-96 (BioSpec, Bartlesville, OK, USA). All samples (300 μL, 0.3 mg total proteins) were subjected to click-chemistry reaction with Desthiobiotin-PEG_3-N_3 (Jena Bioscience, Germany, #CLK-AZ104P4−100; 40 mM in DMSO). Samples were further processed for affinity enrichment with Pierce High-Capacity Streptavidin Agarose Resin (ThermoFisher Scientific, #20359). The captured biotinylated protein solution was mixed with 5 × Laemmli reducing sample buffer and heated at 95 °C for 5 min.

Mass Spectrometry Analysis. Enriched protein samples were stacked into a single band by NuPAGE gel electrophoresis and subjected to in-gel trypsin digestion before mass spectrometry analysis. Peptides were analyzed using an Orbitrap QExactive Plus Mass Spectrometer (ThermoFisher Scientific, San Jose, CA, USA) in data-independent acquisition mode (DIA). Protein identification and quantification were performed using the DIA-NN 1.8 algorithm in combination with the DIAgui package (https://github.com/marseille-proteomique/DIAgui). The mass spectrometry proteomics data have been deposited to the ProteomeXchange Consortium via the PRIDE partner repository under the data set identifier PXD073012.

Plasmid Construction and Cloning

Construction of *S. aureus* pLI50_fabH Strain. All plasmids and primers used in this study are listed in Supporting Information Tables S5 and S6. The construction of the overexpression mutant was performed via a restriction-free approach (Figure S4A) using the pLI50_*hpf* as a template. The final plasmid was transformed into electrocompetent *S. aureus* RN4220 to increase transformation efficiency, purified, and then transformed into electrocompetent *S. aureus* ATCC 25923. Validation of the pLI50_*fabH* mutant was made by PCR amplification and Western blotting (Figure S4B,C).

Statistical Analysis

GraphPad Prism 8 (GraphPad Software, Boston, MA, USA) was used for all statistical analyses, as detailed in each figure legend. Differences were considered significant with calculated *p*-values ≤ 0.05.

ASSOCIATED CONTENT

Supporting Information

The Supporting Information is available free of charge at https://pubs.acs.org/doi/10.1021/acsinfecdis.6c00165.

Detailed protocols regarding chemistry and biological evaluation; Figure S1, Bactericidal effect of **MpPPOX** on *S. aureus* ATCC 25923 planktonic growth; Figure S2, Dose−response activity of **HPOX**, **iBPOX**, and **MpPPOX** against THP-1-derived macrophages; Figure S3, Action of clinically relevant antibiotics on preformed biofilms of *S. aureus* ATCC 25923, either alone or in combination with **HPOX**; Figure S4, Generation of the *S. aureus*-pLI50_*fabH* overexpression strain; Figure S5, In silico molecular docking of the OAX inhibitor inside *S. aureus* FabH active site. Figure S6, NMR spectra of the new **MpP$_{yne}$POX** and **iB$_{yne}$POX** probes (PDF)

https://doi.org/10.1021/acsinfecdis.6c00165
ACS Infect. Dis. XXXX, XXX, XXX−XXX

Target proteins identified after a 24 h culture of *S. aureus* through CC-ABPP by LC-ESI-MS/MS analysis, using **HPOX$_{yne}$**, **iB$_{yne}$POX**, or **MpP$_{yne}$POX** probes; source and resistance profile of *S. aureus* clinical isolates; and list of strains, primers, and plasmids used in this study (XLSX)

AUTHOR INFORMATION

Corresponding Authors

Jean-Michel Bolla − *Aix Marseille Univ, INSERM, SSA, MCT, Marseille 13402 cedex 20, France;* orcid.org/0000-0003-3892-4340; Email: jean-michel.BOLLA@univ-amu.fr

Jean-François Cavalier − *Aix Marseille Univ., CNRS, LISM UMR7255, Marseille 13402 cedex 20, France;* orcid.org/0000-0003-0864-8314; Email: jfcavalier@imm.cnrs.fr

Authors

Emma Forest − *Aix Marseille Univ., CNRS, LISM UMR7255, Marseille 13402 cedex 20, France; Aix Marseille Univ, INSERM, SSA, MCT, Marseille 13402 cedex 20, France*

Jordan Lehoux − *IBMM, Univ Montpellier, CNRS, ENSCM, Montpellier 34060, France*

Léo Faion − *IBMM, Univ Montpellier, CNRS, ENSCM, Montpellier 34060, France*

David Ranava − *Aix Marseille Université, CNRS, BIP UMR7281, Marseille 13402 cedex 20, France*

Virginie Mohymont − *Pharmacologie cellulaire et moléculaire, Louvain Drug Research Institute, Université catholique de Louvain (UCLouvain), Brussels 1200, Belgium*

Thierry Durand − *IBMM, Univ Montpellier, CNRS, ENSCM, Montpellier 34060, France*

Stéphane Audebert − *Aix Marseille Univ, CNRS, INSERM, Institut Paoli-Calmettes, CRCM, Marseille Protéomique, Marseille 13402 cedex 20, France*

Luc Camoin − *Aix Marseille Univ, CNRS, INSERM, Institut Paoli-Calmettes, CRCM, Marseille Protéomique, Marseille 13402 cedex 20, France*

Céline Crauste − *IBMM, Univ Montpellier, CNRS, ENSCM, Montpellier 34060, France;* orcid.org/0000-0002-5714-8749

Stéphane Canaan − *Aix Marseille Univ., CNRS, LISM UMR7255, Marseille 13402 cedex 20, France;* orcid.org/0000-0001-7478-300X

Jean Michel Brunel − *Aix Marseille Univ, INSERM, SSA, MCT, Marseille 13402 cedex 20, France;* orcid.org/0000-0002-9355-8980

Françoise Van Bambeke − *Pharmacologie cellulaire et moléculaire, Louvain Drug Research Institute, Université catholique de Louvain (UCLouvain), Brussels 1200, Belgium*

Complete contact information is available at: https://pubs.acs.org/10.1021/acsinfecdis.6c00165

Author Contributions

J.-M. Bolla and J.-F.C: conceptualization. E.F., S.A., and L.C.: data curation. J.L., L.F., T.D., and C.C.: resources. E.F., V.M., D.R., S.A. and L.C.: investigations. E.F., D.R., S.A., L.C., C.C., F.V.B., J.-M. Bolla and J.-F.C.: formal analysis. E.F. and J.-F.C.: visualization. E.F. and J.-F.C.: writing-original draft. E.F., J.L., L.F., D.R., V.M., T.D., S.A., L.C., C.C., S.C., J.M.B, F.V.B., J.M.B., and J.-F.C.: writing-review and editing. J.M. Brunel and J.-F.C.: supervision. J.M. Bolla and J.-F.C.: funding acquisition. J.M. Bolla and J.-F.C.: validation. J.M. Bolla and J.-F.C.: project administration. All authors have given approval to the final version of the manuscript.

Notes

The authors declare no competing financial interest.

ACKNOWLEDGMENTS

We thank Dr. Jérôme JOSSE (Centre International de Recherche en Infectiologie, Lyon, France) for kindly providing the *S. aureus* SH1000 strain used in this study. This work was supported by the CNRS, INSERM, and Aix Marseille University. Proteomics analyses were done using the mass spectrometry facility of Marseille Proteomics (marseille-proteomique.univ-amu.fr) supported by IBISA (Infrastructures Biologie Santé et Agronomie), Plateforme Technologique Aix-Marseille, the Cancéropôle PACA, the Provence-Alpes-Côte d'Azur Region, the Institut Paoli-Calmettes, Fonds Européen de Développement Regional (FEDER), and Plan Cancer. E.F. PhD fellowship was supported by the Ministère de l'Enseignement Supérieur et de la Recherche Française. E.F. has also received a Research and Travel Grant (ID5404) from the Federation of European Microbiological Society (FEMS). F.V.B. is research director from the Belgian FRS-FNRS.

ABBREVIATIONS

ABP, activity-based probe; ABPP, activity-based protein profiling; au, arbitrary unit; CC-ABPP, click-chemistry activity-based protein profiling; LZD, linezolid; MBEC, minimal biofilm eradication concentration; MBIC, minimal biofilm inhibitory concentration; MIC50/MIC90, compound minimum inhibitory concentration leading to 50% or 90% of growth inhibition; MFX, moxifloxacin; OX, oxadiazolone derivatives; VAN, vancomycin

REFERENCES

(1) Aminov, R. I. A brief history of the antibiotic era: lessons learned and challenges for the future. *Front. Microbiol.* **2010**, *1*, 134.

(2) Cook, M. A.; Wright, G. D. The past, present, and future of antibiotics. *Sci. Transl Med.* **2022**, *14* (657), No. eabo7793.

(3) Naghavi, M.; Vollset, S. E.; Ikuta, K. S.; Swetschinski, L. R.; Gray, A. P.; Wool, E. E.; Aguilar, G. R.; Mestrovic, T.; Smith, G.; Han, C.; Hsu, R. L. Global burden of bacterial antimicrobial resistance 1990−2021: a systematic analysis with forecasts to 2050. *Lancet* **2024**, *404* (10459), 1199−1226.

(4) Tacconelli, E.; Carrara, E.; Savoldi, A.; Harbarth, S.; Mendelson, M.; Monnet, D. L.; Pulcini, C.; Kahlmeter, G.; Kluytmans, J.; Carmeli, Y.; Ouellette, M.; Outterson, K.; Patel, J.; Cavaleri, M.; Cox, E. M.; Houchens, C. R.; Grayson, M. L.; Hansen, P.; Singh, N.; Theuretzbacher, U.; Magrini, N.; Group, W. H. O. P. P. L. W. Discovery, research, and development of new antibiotics: the WHO priority list of antibiotic-resistant bacteria and tuberculosis. *Lancet Infect. Dis.* **2018**, *18* (3), 318−327.

(5) WHO. *WHO bacterial priority pathogens list, 2024: Bacterial pathogens of public health importance to guide research, development and strategies to prevent and control antimicrobial resistance.* https://www.who.int/publications/i/item/9789240093461 (accessed 09 February 2025).

(6) Murray, C. J.; Ikuta, K. S.; Sharara, F.; Swetschinski, L.; Aguilar, G. R.; Gray, A.; Han, C.; Bisignano, C.; Rao, P.; Wool, E.; Johnson, S. C. Global burden of bacterial antimicrobial resistance in 2019: a systematic analysis. *Lancet* **2022**, *399* (10325), 629−655.

(7) Bordi, C.; de Bentzmann, S. Hacking into bacterial biofilms: a new therapeutic challenge. *Ann. Intensive Care* **2011**, *1* (1), 19.

(8) Idrees, M.; Sawant, S.; Karodia, N.; Rahman, A. Staphylococcus aureus Biofilm: Morphology, Genetics, Pathogenesis and Treatment Strategies. *Int. J. Environ. Res. Public Health* **2021**, *18* (14), 7602.

(9) Lewis, K. Riddle of biofilm resistance. *Antimicrob. Agents Chemother.* **2001**, *45* (4), 999−1007.
(10) Tuon, F. F.; Suss, P. H.; Telles, J. P.; Dantas, L. R.; Borges, N. H.; Ribeiro, V. S. T. Antimicrobial Treatment of Staphylococcus aureus Biofilms. *Antibiotics (Basel)* **2023**, *12* (1), 87.
(11) Hall, C. W.; Mah, T. F. Molecular mechanisms of biofilm-based antibiotic resistance and tolerance in pathogenic bacteria. *FEMS Microbiol Rev.* **2017**, *41* (3), 276−301.
(12) Liu, H. Y.; Prentice, E. L.; Webber, M. A. Mechanisms of antimicrobial resistance in biofilms. *npj Antimicrob. Resist.* **2024**, *2* (1), 27.
(13) Michaelis, C.; Grohmann, E. Horizontal Gene Transfer of Antibiotic Resistance Genes in Biofilms. *Antibiotics (Basel)* **2023**, *12* (2), 328.
(14) Molin, S.; Tolker-Nielsen, T. Gene transfer occurs with enhanced efficiency in biofilms and induces enhanced stabilisation of the biofilm structure. *Curr. Opin Biotechnol* **2003**, *14* (3), 255−61.
(15) Uruen, C.; Chopo-Escuin, G.; Tommassen, J.; Mainar-Jaime, R. C.; Arenas, J. Biofilms as Promoters of Bacterial Antibiotic Resistance and Tolerance. *Antibiotics (Basel)* **2021**, *10* (1), 3.
(16) O'Neill, J. *Tackling Drug-Resistant Infections Globally: Final Report and Recommendations. The Review on Antimicrobial Resistance*. Wellcome Trust and HM Government. https://amr-review.org/sites/default/files/160525_Final%20paper_with%20cover.pdf (accessed 30 March 2026).
(17) Brotz-Oesterhelt, H.; Brunner, N. A. How many modes of action should an antibiotic have? *Curr. Opin. Pharmacol.* **2008**, *8* (5), 564−73.
(18) Gray, D. A.; Wenzel, M. Multitarget Approaches against Multiresistant Superbugs. *ACS Infect Dis* **2020**, *6* (6), 1346−1365.
(19) Maharramov, E.; Czikkely, M. S.; Szili, P.; Farkas, Z.; Grezal, G.; Daruka, L.; Kurko, E.; Meszaros, L.; Daraba, A.; Kovacs, T.; Bognar, B.; Juhasz, S.; Papp, B.; Lazar, V.; Pal, C. Exploring the principles behind antibiotics with limited resistance. *Nat. Commun.* **2025**, *16* (1), 1842.
(20) Delorme, V.; Diomande, S. V.; Dedieu, L.; Cavalier, J. F.; Carriere, F.; Kremer, L.; Leclaire, J.; Fotiadu, F.; Canaan, S. MmPPOX inhibits Mycobacterium tuberculosis lipolytic enzymes belonging to the hormone-sensitive lipase family and alters mycobacterial growth. *PLoS One* **2012**, *7* (9), No. e46493.
(21) Cavalier, J. F.; Spilling, C. D.; Durand, T.; Camoin, L.; Canaan, S. Lipolytic enzymes inhibitors: A new way for antibacterial drugs discovery. *Eur. J. Med. Chem.* **2021**, *209*, No. 112908.
(22) Forest, E.; Lehoux, J.; Guy, A.; Durand, T.; Audebert, S.; Camoin, L.; Spilling, C. D.; Crauste, C.; Canaan, S.; Brunel, J. M.; Bolla, J. M.; Cavalier, J. F. The polyamino-isoprenyl enhancer NV716 enables the antibacterial activity of two families of multi-target inhibitors against the ESKAPEE bacterium Enterobacter cloacae. *mLife* **2025**, *4* (3), 259−274.
(23) Madani, A.; Mallick, I.; Guy, A.; Crauste, C.; Durand, T.; Fourquet, P.; Audebert, S.; Camoin, L.; Canaan, S.; Cavalier, J. F. Dissecting the antibacterial activity of oxadiazolone-core derivatives against Mycobacterium abscessus. *PLoS One* **2020**, *15* (9), No. e0238178.
(24) Nguyen, P. C.; Delorme, V.; Benarouche, A.; Guy, A.; Landry, V.; Audebert, S.; Pophillat, M.; Camoin, L.; Crauste, C.; Galano, J. M.; Durand, T.; Brodin, P.; Canaan, S.; Cavalier, J. F. Oxadiazolone derivatives, new promising multi-target inhibitors against M. tuberculosis. *Bioorg Chem.* **2018**, *81*, 414−424.
(25) Bakker, A. T.; Kotsogianni, I.; Mirenda, L.; Straub, V. M.; Avalos, M.; van den Berg, R.; Florea, B. I.; van Wezel, G. P.; Janssen, A. P. A.; Martin, N. I.; van der Stelt, M. Chemical Proteomics Reveals Antibiotic Targets of Oxadiazolones in MRSA. *J. Am. Chem. Soc.* **2023**, *145* (2), 1136−1143.
(26) Jo, J.; Upadhyay, T.; Woods, E. C.; Park, K. W.; Pedowitz, N. J.; Jaworek-Korjakowska, J.; Wang, S.; Valdez, T. A.; Fellner, M.; Bogyo, M. Development of Oxadiazolone Activity-Based Probes Targeting FphE for Specific Detection of Staphylococcus aureus Infections. *J. Am. Chem. Soc.* **2024**, *146* (10), 6880−6892.
(27) Lentz, C. S.; Sheldon, J. R.; Crawford, L. A.; Cooper, R.; Garland, M.; Amieva, M. R.; Weerapana, E.; Skaar, E. P.; Bogyo, M. Identification of a S. aureus virulence factor by activity-based protein profiling (ABPP). *Nat. Chem. Biol.* **2018**, *14* (6), 609−617.
(28) Song, H.; Ao, G. Z.; Li, H. Q. Novel FabH inhibitors: an updated article literature review (July 2012 to June 2013). *Expert Opin Ther Pat* **2014**, *24* (1), 19−27.
(29) Tunney, M. M.; Ramage, G.; Field, T. R.; Moriarty, T. F.; Storey, D. G. Rapid colorimetric assay for antimicrobial susceptibility testing of Pseudomonas aeruginosa. *Antimicrob. Agents Chemother.* **2004**, *48* (5), 1879−81.
(30) Weseler, A.; Geiss, H. K.; Saller, R.; Reichling, J. A novel colorimetric broth microdilution method to determine the minimum inhibitory concentration (MIC) of antibiotics and essential oils against Helicobacter pylori. *Pharmazie* **2005**, *60* (7), 498−502.
(31) O'Neill, A. J. Staphylococcus aureus SH1000 and 8325−4: comparative genome sequences of key laboratory strains in staphylococcal research. *Lett. Appl. Microbiol* **2010**, *51* (3), 358−61.
(32) Patil, M.; Serhii, K.; Garzino, F.; Gobert, Q.; Giorgio, S.; Raimundo, J. M.; Bolla, J. M.; Camplo, M. Synthesis and antimicrobial testing of 5-fluorouracil derivatives. *Arch. Pharm.* **2023**, *356* (7), No. e2300103.
(33) Lathram, W. A.; Radka, C. D. Intracellular survival of Staphylococcus aureus in macrophages during osteomyelitis. *Virulence* **2025**, *16* (1), No. 2553789.
(34) Moldovan, A.; Fraunholz, M. J. In or out: Phagosomal escape of Staphylococcus aureus. *Cell Microbiol* **2019**, *21* (3), No. e12997.
(35) Kubica, M.; Guzik, K.; Koziel, J.; Zarebski, M.; Richter, W.; Gajkowska, B.; Golda, A.; Maciag-Gudowska, A.; Brix, K.; Shaw, L.; Foster, T.; Potempa, J. A potential new pathway for Staphylococcus aureus dissemination: the silent survival of S. aureus phagocytosed by human monocyte-derived macrophages. *PLoS One* **2008**, *3* (1), No. e1409.
(36) Seral, C.; Van Bambeke, F.; Tulkens, P. M. Quantitative analysis of gentamicin, azithromycin, telithromycin, ciprofloxacin, moxifloxacin, and oritavancin (LY333328) activities against intracellular Staphylococcus aureus in mouse J774 macrophages. *Antimicrob. Agents Chemother.* **2003**, *47* (7), 2283−92.
(37) Barcia-Macay, M.; Seral, C.; Mingeot-Leclercq, M. P.; Tulkens, P. M.; Van Bambeke, F. Pharmacodynamic evaluation of the intracellular activities of antibiotics against Staphylococcus aureus in a model of THP-1 macrophages. *Antimicrob. Agents Chemother.* **2006**, *50* (3), 841−51.
(38) Thieme, L.; Hartung, A.; Tramm, K.; Klinger-Strobel, M.; Jandt, K. D.; Makarewicz, O.; Pletz, M. W. MBEC Versus MBIC: the Lack of Differentiation between Biofilm Reducing and Inhibitory Effects as a Current Problem in Biofilm Methodology. *Biol. Proced. Online* **2019**, *21*, 18.
(39) Dunne, W. M., Jr.; Mason, E. O., Jr.; Kaplan, S. L. Diffusion of rifampin and vancomycin through a Staphylococcus epidermidis biofilm. *Antimicrob. Agents Chemother.* **1993**, *37* (12), 2522−6.
(40) Zheng, Z.; Stewart, P. S. Penetration of rifampin through Staphylococcus epidermidis biofilms. *Antimicrob. Agents Chemother.* **2002**, *46* (3), 900−3.
(41) Jefferson, K. K.; Goldmann, D. A.; Pier, G. B. Use of confocal microscopy to analyze the rate of vancomycin penetration through Staphylococcus aureus biofilms. *Antimicrob. Agents Chemother.* **2005**, *49* (6), 2467−73.
(42) Avellan, R.; Sarrazin, M.; Spilling, C. D.; Crauste, C.; Canaan, S.; Cavalier, J.-F., Chapter 11 - Deciphering the physiological role of serine enzymes involved in mycobacterial lipid metabolism using activity-based protein profiling. In *Biology of Mycobacterial Lipids*; Fatima, Z.; Canaan, S., Eds. Academic Press: 2022; pp 235−251. DOI: .
(43) Barelier, S.; Avellan, R.; Gnawali, G. R.; Fourquet, P.; Roig-Zamboni, V.; Poncin, I.; Point, V.; Bourne, Y.; Audebert, S.; Camoin, L.; Spilling, C. D.; Canaan, S.; Cavalier, J. F.; Sulzenbacher, G. Direct capture, inhibition and crystal structure of HsaD (Rv3569c) from M. tuberculosis. *FEBS J.* **2023**, *290* (6), 1563−1582.
(44) Larson, G. Some Aspects of the Chemistry of Alkynylsilanes. *Synthesis* **2018**, *50* (13), 2433−2462.

https://doi.org/10.1021/acsinfecdis.6c00165
ACS Infect. Dis. XXXX, XXX, XXX−XXX

(45) Corey, E. J.; Fuchs, P. L. A synthetic method for formyl→ethynyl conversion (RCHO→RC = CH or RC = CR′). *Tetrahedron Lett.* **1972**, *13* (36), 3769−3772.
(46) Va, P.; Roush, W. R. Total synthesis of amphidinolide E. *J. Am. Chem. Soc.* **2006**, *128* (50), 15960−1.
(47) Allegretti, P. A.; Ferreira, E. M. Vicinal bisheterocyclizations of alkynes via nucleophilic interception of a catalytic platinum carbene. *J. Am. Chem. Soc.* **2013**, *135* (46), 17266−9.
(48) Avellan, R.; Lehoux, J.; Francis, T.; Dargham, T.; Celik, L.; Guy, A.; Poncin, I.; Point, V.; Kremer, L.; Durand, T.; Audebert, S.; Camoin, L.; Spilling, C.; Santucci, P.; Crauste, C.; Canaan, S.; Cavalier, J.-F. Mapping of Mycobacterial Enzymes Involved in Triacylglycerol Accumulation as Intrabacterial Lipid Inclusions Using Activity-Based Multitarget Inhibitor Probes. *ACS Infect. Dis.* **2025**, *11* (6), 1589−1605.
(49) Choi, K. H.; Heath, R. J.; Rock, C. O. beta-ketoacyl-acyl carrier protein synthase III (FabH) is a determining factor in branched-chain fatty acid biosynthesis. *J. Bacteriol.* **2000**, *182* (2), 365−370.
(50) Payne, D. J.; Warren, P. V.; Holmes, D. J.; Ji, Y.; Lonsdale, J. T. Bacterial fatty-acid biosynthesis: a genomics-driven target for antibacterial drug discovery. *Drug Discov Today* **2001**, *6* (10), 537−544.
(51) Bhattacharya, M.; Horswill, A. R. The role of human extracellular matrix proteins in defining Staphylococcus aureus biofilm infections. *FEMS Microbiol. Rev.* **2024**, *48* (1), No. fuae002.
(52) Hofbauer, B.; Vomacka, J.; Stahl, M.; Korotkov, V. S.; Jennings, M. C.; Wuest, W. M.; Sieber, S. A. Dual Inhibitor of Staphylococcus aureus Virulence and Biofilm Attenuates Expression of Major Toxins and Adhesins. *Biochemistry* **2018**, *57* (11), 1814−1820.
(53) Kong, C.; Chee, C. F.; Richter, K.; Thomas, N.; Abd Rahman, N.; Nathan, S. Suppression of Staphylococcus aureus biofilm formation and virulence by a benzimidazole derivative, UM-C162. *Sci. Rep* **2018**, *8* (1), 2758.
(54) Bhattacharya, M.; Berends, E. T. M.; Chan, R.; Schwab, E.; Roy, S.; Sen, C. K.; Torres, V. J.; Wozniak, D. J. Staphylococcus aureus biofilms release leukocidins to elicit extracellular trap formation and evade neutrophil-mediated killing. *Proc. Natl. Acad. Sci. U. S. A.* **2018**, *115* (28), 7416−7421.
(55) Nguyen, M. T.; Luqman, A.; Bitschar, K.; Hertlein, T.; Dick, J.; Ohlsen, K.; Broker, B.; Schittek, B.; Gotz, F. Staphylococcal (phospho)lipases promote biofilm formation and host cell invasion. *Int. J. Med. Microbiol* **2018**, *308* (6), 653−663.
(56) Massimi, I.; Park, E.; Rice, K.; Muller-Esterl, W.; Sauder, D.; McGavin, M. J. Identification of a novel maturation mechanism and restricted substrate specificity for the SspB cysteine protease of *Staphylococcus aureus*. *J. Biol. Chem.* **2002**, *277* (44), 41770−7.
(57) Nikolic, P.; Mudgil, P. The Cell Wall, Cell Membrane and Virulence Factors of Staphylococcus aureus and Their Role in Antibiotic Resistance. *Microorganisms* **2023**, *11* (2), 259.
(58) Rivera, E. S.; Weiss, A.; Migas, L. G.; Freiberg, J. A.; Djambazova, K. V.; Neumann, E. K.; Van de Plas, R.; Spraggins, J. M.; Skaar, E. P.; Caprioli, R. M. Imaging mass spectrometry reveals complex lipid distributions across Staphylococcus aureus biofilm layers. *J. Mass Spectrom Adv. Clin Lab* **2022**, *26*, 36−46.
(59) He, X.; Reynolds, K. A. Purification, characterization, and identification of novel inhibitors of the beta-ketoacyl-acyl carrier protein synthase III (FabH) from Staphylococcus aureus. *Antimicrob. Agents Chemother.* **2002**, *46* (5), 1310−8.
(60) Chaudhuri, R. R.; Allen, A. G.; Owen, P. J.; Shalom, G.; Stone, K.; Harrison, M.; Burgis, T. A.; Lockyer, M.; Garcia-Lara, J.; Foster, S. J.; Pleasance, S. J.; Peters, S. E.; Maskell, D. J.; Charles, I. G. Comprehensive identification of essential Staphylococcus aureus genes using Transposon-Mediated Differential Hybridisation (TMDH). *BMC Genomics* **2009**, *10*, 291.
(61) Jebli, N.; Arfaoui, Y.; Van Hecke, K.; Cavalier, J.-F.; Touil, S. Experimental and computational investigation of Z/E isomerism, X-ray crystal structure and molecular docking study of (2-(hydroxyimino)-cyclohexyl)diphenylphosphine sulfide, a potential antibacterial agent. *J. Mol. Struct.* **2021**, *1229*, No. 129634.
(62) Jebli, N.; Hamimed, S.; Van Hecke, K.; Cavalier, J. F.; Touil, S. Synthesis, Antimicrobial Activity and Molecular Docking Study of Novel alpha-(Diphenylphosphoryl)- and alpha-(Diphenylphosphorothioyl)cycloalkanone Oximes. *Chem. Biodiversity* **2020**, *17* (8), No. e2000217.
(63) Qiu, X.; Choudhry, A. E.; Janson, C. A.; Grooms, M.; Daines, R. A.; Lonsdale, J. T.; Khandekar, S. S. Crystal structure and substrate specificity of the beta-ketoacyl-acyl carrier protein synthase III (FabH) from Staphylococcus aureus. *Protein Sci.* **2005**, *14* (8), 2087−94.
(64) Laskowski, R. A.; Swindells, M. B. LigPlot+: multiple ligand-protein interaction diagrams for drug discovery. *J. Chem. Inf Model* **2011**, *51* (10), 2778−86.

https://doi.org/10.1021/acsinfecdis.6c00165
ACS Infect. Dis. XXXX, XXX, XXX−XXX